Research Square

Preprints are preliminary reports that have not undergone peer review.
They should not be considered conclusive, used to inform clinical practice,
or referenced by the media as validated information.

Blockade of the KRAS-FOSL1 axis elicits DNA damage repair deficiency exploitable with local and systemic genotoxic therapies

Silve Vicent

silvevicent@unav.es

Center for Applied Medical Reseach (CIMA)/University of Navarra https://orcid.org/0000-0002-9457-6881

Connor Welch

Center for Applied Medical Reseach (CIMA)/University of Navarra

Gabriela Novoa-Jaso

Center for Applied Medical Reseach (CIMA)/University of Navarra

Carlos Vasquez-Valencia

Center for Applied Medical Reseach (CIMA)/University of Navarra https://orcid.org/0009-0000-2666-4743

Irati Macaya

Foundation for Applied Medical Research, School of Medicine, University of Navarra
https://orcid.org/0000-0001-5698-6452

Julio Jose Jimenez-Alonso

Center for Applied Medical Reseach (CIMA)/University of Navarra https://orcid.org/0000-0002-2476-2507

Alessia Subrizio

Department of Oncology, Molecular Biotechnology Center, University of Turin

Alejandra Fernández-Lagos

Center for Applied Medical Reseach (CIMA)/University of Navarra

Sofia Llorente

VHIO

Marta Jimenez

CNIO

Rosario Prados-Carvajal

CABIMER

Haritz Moreno

Center for Applied Medical Reseach (CIMA)/University of Navarra

Ines Lopez

Center for Applied Medical Reseach (CIMA)/University of Navarra

Nerea Bakartxo

Center for Applied Medical Reseach (CIMA)/University of Navarra

Jonathan Rub

MSKCC

Andrea Crescencia Domingo Ratia

Center for Applied Medical Reseach (CIMA)/University of Navarra https://orcid.org/0009-0002-9867-1533

Paolo Battuello

Department of Oncology, Molecular Biotechnology Center, University of Torino, Torino, Italy;

Xabier Bujanda-Cundin

Center for Applied Medical Reseach (CIMA)/University of Navarra

Pablo Huertas

Centro Andaluz de Biologia Molecular y Medicina Regenerativa-CABIMER, Universidad de Sevilla-CSIC-Universidad Pablo de Olavide https://orcid.org/0000-0002-1756-4449

Teresa Macaruya

Hospital Clinic

Luis Paz-Ares

H12O-CNIO Lung Cancer Clinical Research Unit

Giovanni Crisafulli

IFOM ETS - The AIRC Institute of Molecular Oncology https://orcid.org/0000-0002-5511-1555

Alfonso Calvo

CIMA-UNAV

Elizabeth Guruceaga

CIMA Universidad de Navarra https://orcid.org/0000-0003-0547-681X

Tuomas Tammela

Memorial Sloan Kettering Cancer Center https://orcid.org/0000-0003-3675-6961

Rafael Martinez-Monge

Clinica Universidad de Navarra

Fernando Lecanda

Center for Applied Medical Research (CIMA)

Alberto Bardelli

IFOM ETS, The AIRC Institute of Molecular Oncology,

Irene Ferrer

Unidad de Investigación Clínica de Cáncer de Pulmón, Instituto de Investigación Hospital 12 de Octubre-CNIO, Madrid

Tian Tian

Vall d'Hebron Institute of Oncology (VHIO)

Mariangela Russo

Department of Oncology, Molecular Biotechnology Center, University of Torino, Torino, Italy.
https://orcid.org/0000-0003-4625-1449

Article

Keywords: KRAS, lung cancer, pancreatic cancer, DNA damage repair, homologous recombination, PARP inhibitor, radiotherapy, drug tolerant cells

Posted Date: March 31st, 2026

DOI: https://doi.org/10.21203/rs.3.rs-9085811/v1

License: This work is licensed under a Creative Commons Attribution 4.0 International License.
Read Full License

Additional Declarations: Yes there is potential Competing Interest. S.V. has received research funding unrelated to this project and consulting fees from Revolution Medicines, additional funding for unrelated work from Roche, Verastem Oncology, and BridgeBio, and is a scientific advisor for Libera Bio. F.L. has received funding for unrelated work from Roche. A.B. reports receipt of grants/research supports from Neophore. A.B. is stock shareholder of Neophore and Kither Biotech. A.B. is advisory boards member for Neophore.

Blockade of the KRAS-FOSL1 axis elicits DNA damage repair deficiency exploitable with local and systemic genotoxic therapies

Connor Welch[1,2,3,16], Gabriela Novoa-Jaso[1,2,3,17], Carlos Vasquez-Valencia[1,17], Irati Macaya[1], Julio José Jimenez-Alonso[1], Alessia Subrizio[4], Alejandra Fernández-Lagos[1], Sofia Llorente[5], Marta Jimenez[2,6], Rosario Prados-Carvajal[8], Haritz Moreno[1], Ines Lopez[1], Nerea Bakartxo[1], Jonathan Rub[9], Andrea C. Domingo[1], Paolo Battuello[4,7], Xabier Bujanda-Cundin[1], Pablo Huertas[8], Teresa Macarulla[5], Luis Paz-Ares[2,6,10,11], Giovanni Crisafulli[7], Alfonso Calvo[1,2,3,12], Elizabet Guruceaga[12,13], Tuomas Tammela[9], Rafael Martinez-Monge[14], Fernando Lecanda[1,2,3,12], Alberto Bardelli[4,7], Irene Ferrer[2,6], Tian V. Tian[5], Mariangela Russo[4, 7], Silve Vicent[1,2,3,12,15*]

1. Solid Tumours Program, Centre for Applied Medical Research (CIMA)-University of Navarra, Pamplona, Spain.

2. Centro de Investigación Biomédica en Red de Cancer (CIBERONC), Madrid, Spain.

3. Department of Pathology, Anatomy and Physiology, University of Navarra, Pamplona, Spain.

4. Department of Oncology, Molecular Biotechnology Center, University of Turin, Turin, Italy.

5. Preclinical and Translational Research Program, Vall d'Hebron Institute of Oncology (VHIO), Barcelona, Spain.

6. H12O-CNIO Lung Cancer Clinical Research Unit, Instituto de Investigación Hospital 12 de Octubre & Centro Nacional de Investigaciones Oncológicas (CNIO), Madrid, Spain.

7. IFOM ETS, The AIRC Institute of Molecular Oncology, Milan, Italy.

8. Centro Andaluz de Biología Molecular y Medicina Regenerativa (CABIMER), Sevilla, Spain.

9. Cancer Biology and Genetics Program, Sloan Kettering Institute, Memorial Sloan Kettering Cancer Center, New York, NY, USA.

10. Medical Oncology Department, Hospital Universitario 12 de Octubre, Madrid, Spain

11. Medical School, Universidad Complutense, Madrid, Spain.

12. Navarra Institute for Health Research (IDISNA), Pamplona, Spain.

13. Bioinformatics Platform, Centre for Applied Medical Research (CIMA)-University of Navarra, Pamplona, Spain.

14. Department of Radiation Oncology, Clínica Universidad de Navarra, Pamplona, Spain.

15. University of Navarra, Pathology, Anatomy and Physiology Department, Pamplona, Spain

16. Current address: Department of Oncology, University of Turin, Turin, Italy.

17. Equal contribution.

*Correspondence to: Silve Vicent; address: 55 PIO XII Avenue, CIMA Building, 31008, Pamplona, SPAIN; phone: +34 948194700 (ext. 812029); email: silvevicent@unav.es

Running title: KRAS blockade sensitizes to genotoxic therapies.

Key Words: KRAS, lung cancer, pancreatic cancer, DNA damage repair, homologous recombination, PARP inhibitor, radiotherapy, drug tolerant cells.

ABSTRACT

The clinical approval of direct KRAS inhibitors represents a milestone in precision oncology. Nonetheless, resistance heterogeneity limits durable clinical responses and impedes the nomination of a ‘‘one-size-fits-all’’ strategy for combination therapies. We circumvent this impasse by uncovering a core vulnerability elicited by KRAS blockade which transcends tissue origin, KRAS mutation, intrinsic KRASi sensitivity, and clinically relevant concurrent mutations. Specifically, we show that KRAS inhibition elicits a functional deficit in DNA damage repair by transcriptionally repressing homologous recombination. This *BRCAness* phenotype constitutes a conditional synthetic lethality to PARP inhibitors and radiotherapy, which synergize with single KRAS blockade and significantly delay the onset of secondary resistance. Integrative analyses identify the transcription factor FOSL1 as an upstream regulator of homologous recombination whose depletion sensitizes to PARP inhibition and radiotherapy. Collectively, we define a translational trajectory for the combination of KRAS inhibitors with clinically approved DNA-damaging agents as a therapeutic strategy treatment potentially expandable to most, if not all, mutant *KRAS* cancers.

INTRODUCTION

Mutant (mut) *KRAS* tumours have historically been treatment-refractory and associated with a dismal prognosis. Direct KRAS inhibitors (KRASi) transformed the treatment, offering single agent therapies to non-small cell lung cancer (NSCLC) patients harbouring KRASG12C mutations[1,2]. Nonetheless, resistance mechanisms rapidly occur across tumor types upon clinical KRAS inhibition[3,4]. Reactivation of RAS signalling via secondary RAS mutations, KRASG12C amplification, KRASG12C switch II binding pocket mutations, dysregulation of upstream receptor tyrosine kinases, mutations in alternative oncogenes and/or tumor suppressor genes (TSGs), or phenotype switching exemplify the plethora of resistant mechanisms appearing on KRASi treatment[3–9]. Such resistance heterogeneity has hindered the implementation of upfront drug combinations capable of yielding meaningful responses across a large fraction of mut *KRAS* cancers. An alternative strategy to rationally nominate drug combinations is to exploit universally conserved vulnerabilities generated upon pharmacological KRAS inhibition with already approved anticancer therapies.

The clinical paradigm of synthetic lethality is the chemical inhibition of PARP by specific inhibitors (PARPi) in cancers with homologous recombination deficiency (HRD) often driven by mutations in genes such as BRCA1 and 2 or epigenetic alterations in HR elements[10–13]. PARP inhibitors 'trap' PARP proteins to single-strand breaks and drive the generation of double-strand breaks (DSBs), ultimately leading to death in cells unable to repair such DSBs such as those with HRD. However, the clinical efficacy of PARP inhibitors to date is constrained to HRD tumors. In other settings, studies have unveiled how tumor cells may rewire DNA machinery in response to pharmacological blockade of actionable oncogenes in a process termed adaptive mutability[14]. This process may be exploited under the concept of 'conditional synthetic lethality' (CSL) by which pharmacological cellular rewiring induces a functional dependency on other signaling axis, whose concomitant inhibition is lethal to tumor cells. Examples of therapy-driven CSL which converge on genome integrity include (i) BRAFi/MEKi provoking a *BRCAness* phenotype in melanoma, exploitable with HDAC3i which elicits transcriptional repression of non-homologous end joining (NHEJ) elements[15]; (ii) EGFRi driving genomic stress, therapeutically leveraged with ATMi to delay

the onset of EGFRi resistance[16]; (iii) MAPKi eliciting global genome instability in melanoma which may be exploited with preclinical DNA-PKcs inhibitors[17]; and (iv) EGFR blockade driving selective sensitivity to REV1 in colorectal cancer[18]. Despite such therapies highlighting nodes of therapeutic intervention, nominated combinatorial partners (ATMi, DNA-PKi, REV1i) are not clinically approved, restricting their clinical relevance. Nomination of clinically approved strategies to leverage therapy-driven DNA rewiring is therefore of paramount importance, particularly in *KRAS*-mutated tumors.

In this study, we identify that KRASi induces a functional deficit in DSB repair governed through a transcriptional loss of homologous recombination (HR) genes BRCA1/2 and RAD51. This phenotype is species-conserved, elicited by both mutant-specific and pan-RAS KRASi across tumours of distinct tissue of origin, independent of KRAS activating mutation, and spans drug-tolerant populations capable of continuing mitotic progression under targeted therapy. KRASi induces a CSL which renders mut *KRAS* NSCLC and PDAC sensitive to the DNA-damaging cancer agents PARPi and radiotherapy (RT) *in vitro* and *in vivo,* whilst maintaining favourable toxicity profiles in preclinical models. Mechanistically, we demonstrate that the *BRCAness* phenotype elicited by KRASi is dependent on a FOSL1 transcriptional circuitry, with FOSL1 depletion abrogating BRCA2/RAD51 expression and sensitizing to PARPi and RT *in vitro* and *in vivo*. Furthermore, clinical datasets correlate high FOSL1 levels to poor prognosis following DSB-inducing therapies. Taken together, our study positions PARPi and RT in combination with KRASi as candidate treatment strategies for patients bearing mut *KRAS* cancers, including the targeting of early KRASi drug-tolerant populations prior to the acquisition of bona fide resistance mechanisms. This outlines a path to clinically evaluate these combination therapies, addressing an unmet need in patients harbouring *KRAS* mutations.

RESULTS

KRAS inhibition disrupts DNA damage repair competency

Postulating that KRAS inhibition may uncover vulnerabilities which could expose potential nodes of therapeutic intervention, we sought to identify early common transcriptional programs elicited by blockade of KRAS signalling which transcended tissue type, species, activating RAS mutation and clinically relevant concurrent mutations. To this end, we first integrated consistently downregulated genes from human NSCLC (H358: *KRAS G12C*) and PDAC (HPAFII: *KRAS G12D*) cells exposed to genetic (shRNA) and pharmacological (sotorasib, MRTX1133) KRAS inhibition (**Fig. 1A and B, and Suppl. Table 1**). We next searched for repressed genes in isogenic mouse NSCLC cells (LKR10: *Kras G12D*) CRISPR-edited to ablate clinically-relevant tumor suppressor genes (TSGs) in NSCLC (i.e., *Trp53*, *Stk11* and *Keap1*) treated with the RAS(ON) multi-selective inhibitor RMC-7977 (**Fig. 1C, Suppl. Fig. 1A, and Suppl. Table 1**). We observed a consistent convergence on mechanisms pertaining to DNA stability such as Fanconi Anemia (FA), HR, mismatch repair (MMR), nucleotide excision repair (NER), and base excision repair (BER) (**Fig. 1D**). A negative enrichment of DDR categories was found in additional human and mouse cell lines from PDAC and cholangiocarcinoma (CCA) under KRASi treatment, as well as in a second panel of TSG CRISPR-edited mouse NSCLC cells (KLA) (**Fig. 1E, Suppl. Fig. 1B, Suppl. Table 2**). Furthermore, mining of publicly available proteomics data sets of NSCLC and PDAC cell lines treated with sotorasib[19] supported the depletion of the DNA damage repair (DDR) pathways, particularly FA and HR, at the protein level (**Suppl. Fig. 1C and D, and Suppl. Table 2**). Taken together, these data indicate that a subset of DDR genes is robustly governed by KRAS oncogenic signalling across cellular models which recapitulate the tissue and genetic heterogeneity seen in patients expressing oncogenic KRAS.

To investigate if the depletion of DDR pathways elicited by KRAS inhibition translates into DNA damage induction, we assessed γH2AX expression as a readout of DSBs induced by a deficiency in the DDR machinery. Immunoblot analysis revealed an increase in γH2AX protein in a KRASi dose-dependent manner across NSCLC (H358 and H2030) and PDAC (MiaPaca2 and HPAFII) cell

lines (**Fig. 1F**). These results were substantiated by a neutral comet assay showing increased presence of DSBs upon KRASi treatment as indicated by the assessment of the tail and olive moment parameters (**Fig. 1G and H**). This data suggests that the functional depletion of oncogenic KRAS signalling favors genome instability.

Local radiotherapy potentiates the anticancer effect of KRASi

We next evaluated if the impaired capability to repair exogenously induced DNA damage under KRASi pressure would expose a synthetic lethality with clinically approved therapies. To this end, we concomitantly treated cancer cells with KRASi and RT, the later causing indiscriminate DNA damage via base, single-strand breaks (SSBs), double-strand breaks (DSBs) and clustered DNA lesions, at doses <IC50. The combination strategy significantly reduced cellular viability in a panel of NSCLC cell lines (H2030, H358, HCC44, SKLU-1) with respect to single treatments, a phenotype which was recapitulated in a PDAC (HPAFII) cell line (**Fig. 2A and B, and Suppl. Fig. 2A**). Reasoning that this phenotype was derived through a therapeutic convergence on DNA stability, we evaluated DNA damage across all treatment arms. Subsequent analysis of γH2AX expression as a surrogate of DSBs revealed that the KRASi and RT combination potently exacerbated the damage in all the models (**Fig. 2C**).

Then we explored if a combination strategy incorporating RT could delay the onset of KRASi resistance, through proving synthetically lethal with the KRASi-induced HR deficiency in drug treatment-tolerant populations. We employed long-term TTP *in vitro* assays using KRASi-intrinsically sensitive (H358, MiaPaca2) and resistant (H2030, SKLU-1, H1792) human NSCLC and PDAC cell lines. The combination demonstrated a potent capability to significantly delay KRASi or RT escape both in NSCLC and PDAC models harbouring both G12C and G12D activating mutations (**Fig. 2D and E, and Suppl. Fig. 2B and C**). Similar results were obtained in primary NSCLC and PDAC cell lines derived from GEM models in which treatment arms exposed to the combination therapy failed to acquire resistance even following >2 months of treatment pressure, despite tumour outgrowth being observed by single-treatment arms (**Fig. 2F, and Suppl. Fig. 2D**).

To test the antitumor effect of the combination therapy *in vivo,* we used KRASi-intrinsically sensitive (H358) and resistant (H2030) NSCLC cell-derived xenografts (CDXs) treated with a KRASi and/or RT. The combined treatment demonstrated a potent anticancer effect, eliciting deep tumor regressions (18 out of 20) whilst zero tumours treated with single treatments exhibited tumour regression (**Fig. 2G-J**). Likewise, treatment of a CDX derived from a *KRAS G12C* PDAC cell line (MiaPaca2) with the combined treatment elicited stronger antitumor responses than single therapies (**Fig. 2K and L**). *In vivo* testing of the combined treatment in mouse tumor cell-derived allografts (CDA) from NSCLC (T1: *KRAS G12C*) and PDAC (511950: *KRAS G12D*) in immunocompetent mice paralleled the CDX findings, with only the combination therapy yielding tumor regressions across both models (**Fig. 2M-P**). Of note, the combined treatment had no effect on mouse body weight (**Suppl. Fig. 2E**). Furthermore, a favourable toxicity profile was observed when evaluating serum markers of liver damage across models (i.e., alkaline phosphatase -ALP-, alanine aminotransferase -ALT-, aspartate aminotransferase -ASP-, albumin, and cholesterol) or blood cell count (i.e., white blood cells, neutrophils, lymphocytes, monocytes, eosinophils, and basophils) in immunocompetent mice (**Suppl. Fig. 2F-I**). Collectively, these findings indicate that the HRD phenotype originated by KRASi can be leveraged with the concomitant addition of RT without adverse side effects in mouse models.

KRASi induces a homologous recombination deficiency state in drug-tolerant populations

We observed HR, a DDR pathway involved in the resolution of DSBs, to be consistently downregulated across human and mouse mut *KRAS* cell lines covering tissue types with a high prevalence of KRAS activating mutations (**Fig. 3A and Suppl. Fig. 3A**). qPCR analysis of central HR components pertaining to either the BRCA complex (i.e., BRCA1/BRCA2) or essential scaffolding proteins (i.e., RAD51), whose individual loss is sufficient to induce HRD, in additional NSCLC (H2030) and PDAC (MiaPaca2) cell lines treated with KRASi revealed a similar expression decrease (**Suppl. Fig. 3B**). KRASi-induced downregulation of key HR proteins in NSCLC (H358 and H2030) and PDAC (MiaPaca2 and HPAFII) occurred in a dose-dependent manner (**Fig. 3B and C**). Furthermore, analysis of tumor cells from single cell RNA-seq data of a mut *Kras* genetically-

engineered mouse (GEM) of NSCLC where KRAS was pharmacologically inhibited for 5 or 20 days using MRTX1133[8] confirmed the early and late inhibition of BRCA1/2 and RAD51 *in vivo* (**Suppl. Fig. 3C and D**). Collectively, these results suggest that KRAS blockade elicits an HRD phenotype across mut *KRAS* cancers.

To evaluate if KRAS inhibition has functional implications on HR activity, we employed a tri-plasmid construct traffic light reporter (TLR) system by which HR-mediated repair of a selectively induced break by SCE-1 results in GFP expression whilst repair by NHEJ yields mCHERRY signal[20]. Here, KRASi abrogated GFP events, indicating depleted HR competency in NSCLC (H2030) and PDAC (MiaPaca2) cell lines (**Fig. 3D**), demonstrating that the downregulation of HR components translates into a functional deficit.

Next, we questioned whether the HRD phenotype is exclusive to the bulk population or may occur in cellular populations capable of maintaining cell cycle progression under KRASi treatment. To do this, we first mined scRNA-seq data of mut *KRAS* NSCLC cells at distinct time points following KRAS inhibition *in vitro*[21]. Projection of individual cells on the basis of cell cycle-related genes unveiled a uniform G_1-arrested population at 24 hours consistent with an overt response to KRAS inhibition. In keeping with the published findings reporting cellular bypass to pharmacological KRAS blockade, a treatment-tolerant cycling cell population was observed at 72 hours posttreatment (**Fig. 3E**). Comparison of cycling (nonG_0/G_1) populations under basal conditions and KRASi treatment revealed decreased expression in BRCA1/2 and RAD51 in cell populations escaping KRASi pressure (**Fig. 3F**). Second, we interrogated *in vivo* scRNA-seq data from the same mut *Kras G12D* GEM NSCLC model exposed to MRTX1133[8]. Analysis of cycling-only cells (nonG_0/G_1) in vehicle vs KRASi-treated mice showed a decrease in the expression levels of BRCA1/2 and RAD51 at 5 and 20 days posttreatment, consistent with the *in vitro* scRNA-seq data (**Suppl. Fig. 3E and F**).

To substantiate the transcriptomics findings of the NSCLC models in other cancer types, we took advantage of a cell cycle reporter plasmid based on a cyclin-dependent-kinase binding-defective p27 mutant (p27K-) which labels quiescent cells in G_0 and G_1 phases and enables isolation of p27K- negative, cycling populations[22] (**Suppl. Fig. 3G**). HPAFII PDAC cells were

transduced with the p27K- plasmid and exposed to vehicle or KRASi for 72 hours. Immunoblot analysis of the cycling populations from vehicle and KRASi-treated HPAFII cells displayed reduced RAD51 protein expression presenting with concomitant increase in γH2AX (**Fig. 3G**), supporting the concept that cycling KRASi-tolerant populations also acquire an HRD phenotype and enhanced genomic instability.

To test whether the HR deficiency can be elicited in human samples after exposure to pharmacological KRAS inhibition, we assessed RNA-seq data from a NSCLC patient treated with sotorasib from which multiple lesions were biopsied pre and posttreatment[23]. To minimize potential differences due to the biopsied tissue, we focused the analysis on the transcriptomics data derived from a common tissue from which several samples were obtained, i.e., the lymph nodes. We observed that expression of HR genes was lower in those samples exposed to sotorasib (**Fig. 3H and Suppl. Table 3**), suggesting that a *BRCAness* phenotype may also be found in tumors from patients treated with KRASi.

KRASi sensitizes mut *KRAS* cancer cells to systemic PARPi blockade

Given the clinical success of PARP inhibitors (PARPi) inducing a synthetic lethality in HR deficient cancers and the possibility for systemic use in patients, we posited that KRASi would also render tumour cells sensitive to PARPi. To this end, we performed cell viability assays to interrogate the effect of combined KRASi and PARPi in NSCLC (H358 and H2030) and PDAC (HPAFII) models and revealed that concurrent KRASi and PARPi blockade elicited a more potent antiproliferative effect than single treatments (**Fig. 4A and B**) with an exacerbated DNA damage found in the drug combination compared to single drugs (**Fig. 4C and Suppl. Fig. 4A**). Second, we tested if the lethality elicited by the combination therapy would delay the acquisition of secondary resistance to KRASi using TTP assays using clinically relevant concentrations of KRASi or PARPi. The addition of PARPi significantly delayed the onset of resistance in NSCLC (H358, SKLU-1, H2030, and H1792) and PDAC (MiaPaca2) models irrespective of the mut allele-specific KRASi or tissue of origin (**Fig. 4D-F and Suppl. Fig. 4B and C**). This salient combinatorial effect extended to mouse cells (**Suppl. Fig. 4D**), underscoring the species-conserved HRD-vulnerability elicited by KRASi.

We next assessed the effect of this combination in other tumours harbouring *KRAS* mutations such as colorectal cancer (CRC). Given that KRAS inhibition alone is insufficient to elicit MAPK blockade due to early upregulation of EGFR activity driving compensatory MAPK signalling through wild-type RAS proteins in CRC[24], dual KRAS and EGFR blockade was utilized for maximal vertical suppression of RAS signalling and abrogation of HR proteins. Combined KRASi and EGFRi treatment of CRC cells (LS513, RW7213, and C106) overtly decreased both BRCA2 and RAD51 protein levels (**Suppl. Fig. 4E**). Supporting the NSCLC and PDAC data, the incorporation of PARPi to a dual KRASi plus EGFRi regimen significantly delayed or abrogated relapse (**Fig. 4G and Suppl. Fig. 4F and G**), confirming the translatability of our combination therapy to other mut *KRAS*-addicted tumours.

To evaluate the anticancer activity of the combination regimen *in vivo*, we first employed two NSCLC CDX models. KRASG12Ci monotherapy mostly induced delayed tumor progression in H358- and H2030-derived tumors. In contrast, PARPi alone failed to elicit antitumour activity compared to the control group, consistent with the intrinsic HR competency of these tumour models. However, the drug combination elicited pronounced tumor regression (H358: 10/10; H2030: 6/9) or stasis in both models (**Fig. 4H-K**). Likewise, the drug combination elicited superior antitumor responses compared to single treatments in two PDAC CDX models utilizing either KRASG12Ci or KRASG12Di (**Fig. 4L-O**). These results were mirrored in 2 allografts in immunocompetent mice (T1 and 511959), spanning 2 tissue types (NSCLC and PDAC) and 2 distinct KRAS mutations (G12C and G12D) (**Suppl. Fig. 4H-K**).

Since KRASi and PARPi are already approved for clinical use, and considering the translational potential of the drug combination, we evaluated the combination therapy in a patient-derived xenograft (PDX) PDAC model. Whilst treatment with a KRASG12Di elicited tumour control, the combination with a PARPi yielded potent tumour regressions, supporting the concept that PARPi can leverage a CSL elicited by KRASi in preclinical models (**Fig. 4P and Q**). Analysis of toxicity parameters including mouse body weight and liver damage biochemical markers in response to single and combined treatments involving sotorasib or MRTX1133 revealed no changes (**Suppl.**

Fig. 4L and M). Taken together, a KRASi-induced HRD can be capitalized upon by therapeutically combining with PARPi.

FOSL1 represents a transcriptional node connecting KRAS to the HR pathway

Having demonstrated the potential of combining KRASi with DNA-damaging therapies for the treatment of mut *KRAS* cancers, we aimed to identify potential transcriptional nodes downstream of KRAS involved in the regulation of the HR pathway. To achieve this, we established a two-tiered approach (**Fig. 5A and Suppl. Table 4**). First, commonly KRAS-downregulated genes obtained from either NSCLC or PDAC undergoing pharmacological or genetic KRAS inhibition (Log_2FC <-0.5, P<0.05) were queried against a previously published genome-wide CRISPR screen to identify PARPi sensitizers among KRAS-regulated genes[25]. One hundred and one genes in NSCLC and 71 in PDAC were identified to be downregulated upon KRASi and previously described to confer sensitivity to PARPi. Of note, BRCA2 and RAD51 were included in our PARPi sensitizing gene set (**Fig. 5B and C**), underscoring the validity of our candidate selection pipeline in identifying genes conferring sensitivity to PARPi.

Second, the PARPi sensitizing gene sets were then used as input in the CMap (clue.io)[26] to predict potential upstream nodes whose inhibition decreases the expression of the input gene signature. Genes with a connectivity score >90 were subsequently filtered through both transcriptomic datasets generated upon KRAS inhibition as the PARPi sensitizing genes were obtained from a CRISPR screen in wild type *KRAS* cells. This led to the identification of 5 potential regulatory nodes common to NSCLC and PDAC: EZH2, FOSL1, FOXA2, c-MYC and TIP13 (**Fig. 5D and E**). We focused on FOSL1, a *bona fide* effector of oncogenic KRAS across different cancer types[27,28], given that a link to HR regulation was yet to be determined.

To explore the potential relationship of FOSL1 and PARPi, we interrogated RNAseq data from NSCLC (H358) cells expressing a Tetracycline-inducible FOSL1 shRNA (TET-FOSL1sh)[29,30]. We found that the gene set of PARPi sensitizing genes used as input in the CMap analysis was negatively enriched in FOSL1-depleted cells (**Fig. 5F**). In addition, transcriptional repression of HR genes was found in H358 cells expressing the TET-FOSL1sh (**Fig. 5G**). To substantiate the

transcriptomic findings, we assessed RAD51 protein expression in NSCLC (H358) and PDAC (MiaPaca2) cell lines where FOSL1 was depleted using two independent TET-inducible FOSL1 shRNAs, and found a consistent RAD51 decrease in the two models (**Fig. 5H and I**). Taking together, these data underscore a connection between the transcription factor FOSL1 and the DNA damage repair machinery.

FOSL1 inhibition renders *mut KRAS* cancers sensitive to DNA damaging therapies

The previous results led us to investigate the functional role of FOSL1 in the sensitivity to DSB-inducing therapies. We first queried data from the Genomics of Drug Sensitivity in Cancer (GDSC) using ROC plotter[31] and identified that FOSL1 gene expression levels in NSCLC cell lines discriminated responder and non-responder status against olaparib (ROC P-value: 3.4e-5) (**Fig. 6A**). Similar results were observed with additional PARPi such as niraparib and talazoparib (ROC P-value: 3.2e-4 and 9.6e-4 respectively) (**Suppl. Fig. 5A and B**).

Next, we directly tested if FOSL1 inhibition would elicit a state of HRD which would phenocopy KRASi and be therapeutically leveraged using PARPi. To do this, we implemented a TTP assay using NSCLC (H358) and PDAC (HPAFII) cells expressing a TET-FOSL1sh treated with vehicle (control), doxycycline, PARPi, or doxycycline plus PARPi. We observed that whilst doxycycline-induced FOSL1 loss elicited a potent cytotoxic effect as previously reported[27], the combination of FOSL1 ablation and PARPi therapy generated cytotoxic effects in the combination group with regard to the group treated with doxycycline alone (**Fig. 6B and C**). FOSL1 inhibition was sustained throughout the duration of the TTP experiment (**Suppl. Fig 5C**). Complementarily, the effect of FOSL1 genetic loss on the *in vitro* cancer cell relapse was mimicked in both NSCLC (H358) and PDAC (HPAFII) cell lines with an orthogonal approach using an AP-1/FOSL1 inhibitor (AP-1/FOSL1i) (**Fig. 6D and E**).

To investigate the contribution of FOSL1 depletion to PARPi in an *in vivo* setting, CDX from H358 TET-FOSL1sh cells were generated and treated with doxycycline, PARPi or both. Genetic removal of FOSL1 resulted in delayed tumor growth, consistent with previous studies[27]. Furthermore, the combination of FOSL1 genetic silencing and PARPi therapy significantly increased

antitumour responses by experiment endpoint whilst tumour outgrowth was observed in single-treatment arms (**Fig. 6F**). Notably, similar results were observed when RT was used in combination with FOSL1 genetic inhibition (**Fig. 6G**).

Lastly, we tested the prognostic value of FOSL1 in the context of DSB-inducing therapies. Using KM Plotter, we evaluated a cohort of NSCLC patients treated with RT or RT-chemotherapy (CT) and queried survival in function of FOSL1 levels. High FOSL1 levels correlated with significantly worse overall survival (25 vs 51 months respectively; Logrank P = 0.019) (**Fig. 6H**). However, no association with survival was found in NSCLC patients treated exclusively with CT in which double-strand breaks is not the primary mechanism of action, supporting DSB-tied specific role of FOSL1 in genome stability (**Suppl. Fig. 5D**).

Taken together, these data provide a mechanistic link between oncogenic KRAS and HR competency via FOSL1 (**Fig. 6I**).

DISCUSSION

The approval of KRASG12Ci for the treatment of mut *KRAS* cancers represented a landmark in the clinical management of a largely treatment-refractory patient population. Since then, a wealth of clinical and preclinical data has demonstrated that KRAS inhibitors will require their combination with other anticancer agents to achieve curative, long-lasting, responses in patients. However, the selection of drug combination strategies to cover the largest fraction of mut *KRAS* patients has been compromised by the diverse resistant mechanisms emerging upon KRAS inhibitor treatment. In this study, in lieu of nominating a combination therapy intrinsically tied to a specific resistance mechanism, we robustly define a potent vulnerability (not circumscribed to tissue type or KRAS mutation) driven by KRAS inhibition: the tumour-specific depletion of the DDR machinery. These observations nominate the use of two clinically approved therapies, PARPi and RT, as treatment partners with KRASi which could be generalizable across mut *KRAS* cancers. The clinical translation of these therapy combinations is owed to our discovery that a HRD-phenotype is generated in both drug-sensitive and tolerant cancer populations which, as exemplified by the *in vitro* and *in vivo* data, results in more durable responses when combined with PARPi or RT. Furthermore, the mutant-specificity of KRAS inhibitors constrains the HRD-phenotype to only cells harbouring actionable KRAS mutations, conceptually minimizing combination therapy-driven toxicity in non-malignant tissue.

PARPi therapy in HR-deficient tumours arguably represents the most successful example to date of exploiting synthetic lethality for cancer therapy to date[32,33]. Nonetheless, such therapy is limited to cancers harbouring BRCA mutations or HRD such as those of the ovary, breast, prostate and pancreas[10–13]. The findings that KRASi can generate a conditional synthetic lethality by specifically depleting tumoral HR gene levels span the applicability of PARPi to a larger cancer patient population. Our findings are in tune with previous studies capitalizing on the generation of a genetically- or chemically-induced HRD to potentiate PARPi in BRCA-proficient cancers. In human PDAC, *OFD1* regulates *BRCA1* in cell lines and specimens, and its genetic depletion sensitizes to PARPi[34]. In ovarian cancer, a VEGFRi or a MEKi can suppress the expression of HR proteins also

leading to PARPi sensitization[35,36]. While these observations suggest that alternative strategies inducing an HRD phenotype may enable combinations with PARPi or other therapies generating DSBs (i.e., RT) irrespective of the presence of KRAS mutations, the therapeutic window for some of the combinatorial partners is compromised by their high toxicity as monotherapy agents, a limitation that the use of mut KRAS allele-specific inhibitors may circumvent.

Despite the strong anticancer effect of the KRASi plus PARPi (or RT), in most of the tested models tumors eventually develop resistance to the combined treatment. While we have not formally investigated the resistance mechanisms underlying cancer progression to the drug combinations, studies in *BRCA*-mutated cancers under PARPi treatment point to alternative mechanisms of DSBs repair. Pharmacological blockade of Polθ (*POLQ*), which repairs resected DSBs via theta-mediated end joining (TMEJ), is synthetic lethal in BRCA-mutated cancers and targets PARPi resistance[37]. Furthermore, BRCA2 and PALB2 reversions yielding PARPi resistance in prostate cancer present signs of TMEJ repair, implicating Polθ in the drug refractory phenotype[38]. Thus, inhibition of alternative DSBs repair pathways such as TMEJ may be considered in the design of novel combination strategies involving PARPi. Since resistance to RT also involves upregulation of DSBs repair mechanisms[39], concomitant inhibition of those pathways compensating for HRD should also be taken into consideration should the combination of KRASi + PARP/RT in the clinical setting not prove curative.

Mechanistically, our *in silico* and experimental data suggests that KRAS-mediated HR governance is in part dependent on the transcription factor FOSL1. FOSL1 has been previously reported as a KRAS oncogene vulnerability in NSCLC and PDAC, regulating genes involved in G2/M transition[27], but a link to the DDR machinery had not been previously reported. Nonetheless, whether this new functional context for FOSL1 in mut *KRAS* cancers is expandable to other tumor types remains to be determined. Supporting this possibility, previous observations have shown that FOSL1 expression is upregulated in triple negative breast cancer in response to PARPi treatment *in vitro* [40], suggesting a potential pan-cancer role for FOSL1 in the regulation of HR genes.

This work unveils an unappreciated node of therapeutic intervention in KRAS inhibitor biology. Specifically, how KRASG12Ci/G12Di blockade functionally abrogates tumoral HR gene levels and elicits HRD in NSCLC and PDAC which may be leveraged with PARPi and RT. The fact that different KRASi targeting distinct mut *KRAS* alleles yield a similar anti-tumour effect is of particular importance, as next-generation pan-KRASi may extend the reach of these findings beyond tumours harbouring G12C or G12D mutations[41,42]. In addition, our study indicates this feature to be a core characteristic of KRAS inhibition, and thus we foresee a translation of our phenotype to other KRAS-driven tumors. Nevertheless, as this CSL relies on inhibition of RAS signaling, those tumors with a propensity to enact compensatory mechanisms to restore the RAS-MAPK cascade may require more complex combinatorial strategies (e.g., dual EGFRi plus KRASi as we describe in CRC) to maximally induce vertical suppression of MAPK signaling and elicit this HRD-driven vulnerability.

In summary, our study underscores the paradigm that KRAS inhibition engenders an HRD state, and is a core-feature of KRAS biology, transcending tissue of origin, species and *KRAS* activating mutation. Therefore, it defines a mechanism-informed path to capitalize upon KRASi-elicited tumoral HRD to augment anti-tumor efficacy for tumors with an unmet clinical need.

METHODS

Cell lines

NSCLC cell lines (NCI-H1792, NCI-H358, NCI-HCC44, NCI-H2030, and SKLU-1) were cultured in RPMI. NSCLC (LKR10, KLA and T1), PDAC (MiaPaca2, HPAFII, 511950 and FC1242), CCA (KKU-213A, HUCCT1 and KPch) and CRC (C106, RW7213, LS513) cell lines were cultured in DMEM. All media was supplemented with 10% FBS (Gibco), 1% penicillin-streptomycin (Gibco). All lines were sourced from ATCC. T1 cells were kindly provided by Mariano Barbacid and Matthias Drosten (CNIO, Spain). Lines were cultured at 37 °C, 5% CO_2, and medium replenished every 2-3 days. For passaging, cell monolayers were washed with PBS, incubated with trypsin for 5-7 minutes, neutralized in 2x volume of trypsin with complete culture media, centrifuged 1,200 rpm for 5 minutes, supernatant removed and seeded in 10 ml of media. Sample identity was authenticated internally within CIMA's Genomics Unit using Short Tandem Repeat (STR) profiling (AmpFLSTR Identifier Plus PCR Amplification Kit) and frequently tested for mycoplasma (Lonza). Only mycoplasma-negative samples were used for experiments. Samples were stored for short-term (<1 year) in -80 °C, or long-term (>1 year) in liquid nitrogen (-196 °C). TET-inducible shRNA systems (TET-KRASsh, TET-FOSL1sh8 and TET-FOSL1sh10) were described before[30]. For experiments with TET-inducible shRNAs, FBS was substituted for Fetal Clone Serum to prevent off-target induction of the plasmid by residual tetracycline analogues in the serum.

Drugs

Sotorasib, olaparib and MRTX1133 were purchased from MedChem, and RMC-7977 was provided by Jingjing Jiang at Revolution Medicines.

Neutral comet assay method

To assess DNA damage at the level of double-strand breaks (DSBs), a neutral comet assay was performed using the CometAssay® Silver Kit (Ref. 4250-050-K, R&D Systems), following the manufacturer's instructions with minor modifications.

- Cell preparation and treatment. H2030, HPAFII, and H358 cell lines were seeded in 100-mm dishes at densities of 4.5×10^5, 2×10^6, and 3×10^6 cells, respectively, and incubated overnight at 37 °C

with 5% CO_2.The following day, cells were treated with a KRAS inhibitor (KRASi) at line-specific concentrations: 150 nM sotorasib for H2030, 50 nM MRTX1133 for HPAFII, and 50 nM sotorasib for H358. Treatments were maintained for 48 h prior to performing the comet assay. After treatment, cells were resuspended in 1X PBS to a final concentration of 1 x 10^5 cells/mL.

- Slide preparation. Low-melting-point agarose (LMAgarose) was melted by heating in boiling water and maintained at 37 °C until use. For each experimental condition, 10 µL of the cell suspension was mixed with 100 µL of molten agarose, and 50 µL of this mixture was immediately dispensed onto pretreated microscope slides, fully covering the designated area. Slides were incubated at 4 °C, protected from light, for 30 min to allow complete agarose solidification.

- Cell lysis. Once the agarose had solidified, slides were carefully immersed in pre-chilled lysis solution and incubated overnight at 4 °C in the dark to remove cellular membranes and proteins and to release DNA nucleoids.

- Electrophoresis under neutral conditions. Following lysis, slides were equilibrated in 1× neutral electrophoresis buffer for 30 min. Slides were then placed in the electrophoresis chamber with the label oriented toward the cathode and covered with electrophoresis buffer, ensuring that the buffer level did not exceed 0.5 cm above the slides. Electrophoresis was performed at 21 V (approximately 1 V/cm) for 45 min at room temperature.

- DNA precipitation and dehydration. After electrophoresis, slides were incubated in DNA precipitation solution for 30 min at room temperature, followed by incubation in 70% ethanol for 30 min. Slides were then dried in an oven at 37 °C until complete dehydration.

- Staining and mounting. DNA was stained by incubating each agarose area with 100 µL of SYBR™ Gold diluted in TE buffer for 30 min at room temperature in the dark. After gentle washing with deionized water, slides were dried again at 37 °C and mounted using DAKO mounting medium. Slides were stored at 4 °C until analysis.

- Image acquisition and analysis. Images were acquired using a fluorescence microscope equipped with ZEN 3.0 Blue software (ZEISS). Files were initially generated in CZI format and subsequently converted to JPG to enable analysis, as required by the quantification software. Image acquisition

and conversion parameters were kept constant across all experimental conditions. DNA damage was quantified using the OpenComet plugin in ImageJ (National Institutes of Health), which provides multiple quantitative comet assay parameters. Tail Moment and Olive Tail Moment were specifically used for analysis and graphical representation. For each experimental condition, at least 50–100 cells were analyzed. Single-cell data were pooled by experimental condition for subsequent statistical analysis.

P27 system

The pCDH-EF1-mVenus-p27K$^-$ plasmid (Addgene; plasmid #176651) was co-transfected with the packaging plasmids psPAX2 and pMD2.G for lentiviral production. 1.2 x 10^5 H358 and HPAFII cells were infected with lentiviruses and selection was initiated by adding puromycin (5 µg/mL). H358 and HPAFII cell lines stably expressing the mVenus-p27K$^-$ reporter were treated with a KRASi (sotorasib: 100 nM; MRTX11233: 500 nM) for 72 h prior to cell sorting. Cell sorting was performed to specifically isolate the mVenus-low (cycling) population, which was processed for protein extraction and immunoblot analysis.

Traffic Light Reporter (TLR)

TLR assay was implemented as described previously[20]. Plasmids I-SCE1-T2A-IFP, donor-T2A-BFP and the Traffic Light Reporter (TLR) were sourced from Addgene. Briefly, the SCE1 endonuclease introduces a DSB in the TLR construct. HR-directed repair using the donor template results in a functional GFP construct. Mutagenic repair by NJEM/MMEJ results in a frame-shift and the generation of a functional mCherry construct. We stably transduced cell lines with the TLR with an MOI<1 followed by a subsequent transduction with the donor construct. Finally, cells were infected with the I-SCE1-T2A-IFT construct and simultaneously treated with either DMSO or KRASi. Following 72 hours, cells were sorted by flow cytometry and populations quantified (HR events: BFP$^+$IFP$^+$GFP$^+$) and normalized to events in the vehicle condition per each independent experiment.

Time-to-progression (TTP) assays

Between 5-10 x 10^6 cells were seeded per 100 cm^2 plate, 24 hours later media was supplemented with either control (DMSO) or single/combination therapies. On day 3, cells were

trypsinized, counted and replated. Cells were then counted once a week. Counts reported as 0 reflect time points in which viable cells could not be counted due to insufficient material present. In such cases, the medium was changed as stated above and samples were trypsinized and counted when sufficient material was available. For TTPs with radiotherapy, plates were irradiated 24 hours after seeding using a Nordon Gamma3000 Irradiator.

Western Blotting

Culture plates were washed with PBS and cells were scraped in lysis buffer (1% NP-40, 150 mM NaCl, 50 mM Tris pH 7.4, 1 mM EDTA, 1% glycerol, 25mM sodium fluoride, 1mM sodium orthovanadate, and supplemented with protease inhibitor cocktail -Roche-). They were incubated for 1 hour on ice with frequent agitation by vortex. Protein samples were resolved by SDS PAGE and transferred to nitrocellulose membranes (BioRad) and incubated in 5% milk TBS-T for 1 h prior to the addition of primary antibody. Antibodies used were: BRCA2 (1:1000, #10741, CST), BRCA1 (1:200, #Sc-6954 (D-9), Santa Cruz Biotechnology), RAD51 (1:1000, #8875, CST), Phospho-Histone H2A.X-Ser139 (1:1000, #9718 (20E3), CST), FOSL1: (1:1000, #5281 (D80B4), CST), LKB1 (1:500, #3047 (D60C5), CST), KEAP1 (1:500, #4678 (P586), CTS), P53 (1:1000, #2524 (1C12), CST), HSP90 (1:500, #Sc-69703, Santa Cruz Biotechnology), β-Actin: (1:5000, #A5441, Sigma), β-Tubulin (1.1000, #Sc-9104 (H-235), Santa Cruz Biotechnology), GAPDH (1:1000, #5174, CST), Vinculin (1:1000, #13901 (E1E9V), CST).

Membranes were washed, incubated with secondary antibody (1:5,000), and incubated with peroxidase substrate Super-Signal West Pico Reagent (ThermoFisher). Image capture was completed using a Chemidoc MP Imaging System.

***In vivo* experiments**

All animal experimentation was completed under the approval of the institutional animal care committee of the University of Navarra or the Vall d'Hebron institute of oncology (VHIO) under the protocols CEEA/065-23 and 2020.010 respectively. Mice were housed in a 12-h gradient light/dark schedule to mimic the dawn/twilight cycle, maintained at 20-24 °C with humidity ranges of 50% (+/-10%) and cared for by the Animal Facility staff at CIMA or VHIO. Immunocompromised (Rag2-/-;

Il2γr-/- (Jackson Laboratories) for CDX, and Balb-C$^{nu/nu}$ for PDX) were housed in positive pressure cages. Immunocompetent mice used were F1 (C57Bl/6J x 129S4/Sv), with parental strains procured from Janvier.

Subcutaneous xenograft studies

For cell-derived xenograft (CDX) and allograft (CDA) implantation, between 1 x 10^6 to 5 x 10^6 cells were resuspended in 100 µl of PBS with 50% Matrigel (Corning). Cells were implanted into the left and right flanks. For patient-derived xenografts (PDX) 1 mm^3 pieces were subcutaneously implanted. Tumours were measured with a digital calibre. Once tumours averaged 100-150 mm^3, mice were randomized, and treatment was initiated. Tumour volume was measured every 3-4 days following treatment start using the following formula: volume= π/6 x length x $width^2$.

Drug treatment studies

For subcutaneous experiments (CDX, CDA or PDX) drug doses were as follows. Control groups were treated with corn oil supplemented with 10% DMSO. The administration route was as follows: sotorasib (p.o. qd 10 mg/kg or 30 mg/kg), olaparib (p.o. qd 50 mg/kg or 100 mg/kg), MRTX1133 (i.p. bid 3 mg/kg or 10 mg/kg). Sotorasib and Olaparib was resuspended in 10% DMSO in corn oil, MRTX1133 was resuspended in 10% DMSO-40% PEG300-5% Tween-80-45% Saline. For experiments involving TET-inducible systems, mice were fed 2 mg/mL doxycycline plus 5% sucrose in drinking water which was replenished every 2-3 days.

Radiotherapy

2-3 h following treatment initiation, tumours were irradiated using the small animal radiation research platform (SARRP, Xstrahl) consisting of a 220kV dual-focus X-ray tube. A single dose of 15 Gy (H358, MiaPaca2, 511950) or 20 Gy (T1, H2030) was administered to the tumour centre as confirmed by radiation dosimetry curves. Tumours were isolated from the mice body with a clip to stabilize the desired irradiated region and a U-computer tomography (µCT) scan was taken for the most representative tumour of each experiment. This was used as input for muriplan to ensure the desired radiation dosage to the tumour region using Montecarlo calculations.

Toxicity Studies

At the experiment endpoint, approximately 500 µL blood was extracted through cheek stab from a minimum of 3 mice per group. Samples were passed through the Hemavet 950 counter (Drew Scientific Inc) to analyse full blood count (white blood cells, WBC), erythrocytes, and leukocytes (Monocytes, neutrophils, basophils, lymphocytes). Following this, samples were centrifuged at 2,000 g for 5 min and blood serum was transferred to a new tube. The sample was subsequently passed through a COBAS 6000® Analyser to characterise the following markers of abnormal liver function Albumin (ALB), alkaline phosphatase (ALP), alanine aminotransferase (ALT), aspartate aminotransferase (AST), and cholesterol.

***In silico* drug sensitivity**

In vitro drug sensitivity of indicated drugs was derived using the ROC plotter on lung cancer cell lines, specifically calculating responses based on lower and upper tertiles of IC_{50}[43]. Datasets available were derived from the GDSC2 (Genomics of Drug Sensitivity in Cancer 2).

Survival analysis

Survival plots pertaining to FOSL1 overall survival were extracted from KM plotter (kmplot.com). Patients were segregated by median FOSL1 levels, all patients who had received radiotherapy irrespective of concomitant treatment regiments were included in the analysis. No filters were applied regarding tumour staging, gender, smoking history nor histological features of the tumour.

RNA sequencing Data

Total RNA was measured using BioAnalyzer and then treated with Dynabeads mRNA purification kit (Invitrogen) which uses polyT beads to bind the polyA tail present on eukaryotic mRNAs. Then, the library preparation step is performed with MGIEasy Fast RNA Library preparation kit using the mRNA captured previously and following steps are: RNA fragmentation, reverse transcription, second strand synthesis and end repair, adapter ligation, circularization and DNB-seq preparation. Before the sequencing step, libraries were checked using the BioAnalyzer platform. The sequencing was done using DNBSEQG4000 platform (MGI) and the output generated was around 70 M reads/sample with 150PE read configuration.

RNA-seq analysis was done following protocols described earlier[58]. First, gene expression data was normalized with edgeR[59] and voom[60]. After quality assessment and outlier detection using R/Bioconductor[44], a filtering process was performed. Genes with read counts lower than 6 in more than 50% of the samples of all the studied conditions were considered as not expressed in the experiment under study. LIMMA (Linear Models for Microarray Data)[45] was used to identify the genes with significant differential expression between experimental conditions. Genes were selected as differentially expressed using a B > 0. Further functional and clustering analyses and graphical representations were performed using R/Bioconductor[44].

Analysis of biological pathways from RNA-seq data was performed using Gene Ontology at ShinyGO[46].

Single Cell RNA-seq data

Single cell RNA-seq data of H358 treated with a KRASi (ARS-1620) for 0, 24 and 72 h was reported previously[21]. Raw scRNA-seq counts from controls and treated replicates were merged into a single count matrix. Following the original authors' results metadata, doublets were excluded, and cells were assigned to their respective biological samples. Data filtering, high variable gene selection and both linear and non-linear dimensional reduction were performed as described previously[21]. Data dimensional projection was selected to discriminate cellular subpopulations with distinct cell cycle transcriptional signatures. BRCA1, BRCA2 and RAD51 reads were retrieved from time points 0 h and 72 h by capturing only cellular subpopulations expressing S-G_2/M transcriptional signatures.

Single cell RNA-seq of a KrasG12D NSCLC mouse model treated with a KRASi (MRTX1133) for 5 or 20 days[8]. Raw scRNA-seq counts from controls and treated replicates were merged into a single count matrix. Following the original authors' results metadata, doublets were excluded, and cells were assigned to their respective biological samples. Data filtering, high variable gene selection and both linear and non-linear dimensional reduction were performed as described previously[8]. To categorise cells by their cycling status, we used the CellCycleScoring function from the Seurat package (v5.3.1)[47]. Each cell was assigned a score based on the expression of S and G_2/M phase

markers. According to these scores, cells were assigned to G_1, S or G_2/M. For downstream analyses, cells in the S and G_2/M phases were classified as proliferative, whereas those in G1 were classified as non-proliferative. To identify differentially expressed genes between conditions, pseudobulk analysis was performed using DESeq2 (v 1.50.2)[48]. Raw counts were aggregated by biological replicate and proliferative state, and the data were normalised using the vst (Variance Stabilising Transformation) function from the DESeq2 package. Finally, differential gene expression was computed between groups, and results were visualised using ggplot2 v(4.0.1)[49].

Statistics

Sample size was chosen using www.biomath.info/power/ttest.htm or based on similar experiments previously published by the authors. For comparison of two groups, normality (Shapiro–Wilk test) and variance (Levene test) was assessed. Groups with normal distribution followed a t-test. Non-normal samples were analysed using a Mann-Whitney test (equal variances) or a Median test (unequal variances). For comparison of more than two groups, a residual test was performed to study normality and Levene test assessed homoscedasticity. ANOVA, Brown Forsythe, Kruskal Wallis or Median tests were performed depending on data distribution. A post-hoc test (Dunnet) explored paired comparisons. All analyses were two-tailed. Error bars correspond to either standard deviation (S.D.) or standard error of the mean (S.E.M). Survival analyses were done using the Log-rank test. Statistical analyses were done with GraphPad software v8.

REFERENCES

1. Skoulidis, F. *et al.* Sotorasib for Lung Cancers with KRAS p.G12C Mutation . *N. Engl. J. Med.* **384**, (2021).
2. Jänne, P. A. *et al.* Adagrasib in Non-Small-Cell Lung Cancer Harboring a KRASG12C Mutation. *N. Engl. J. Med.* 1–12 (2022) doi:10.1056/NEJMoa2204619.
3. Awad, M. M. *et al.* Acquired Resistance to KRAS G12C Inhibition in Cancer . *N. Engl. J. Med.* **384**, (2021).
4. Dilly, J. *et al.* Mechanisms of Resistance to Oncogenic KRAS Inhibition in Pancreatic

Cancer. *Cancer Discov.* **14**, 2135–2161 (2024).

5. Ryan, M. B. *et al.* Vertical pathway inhibition overcomes adaptive feedback resistance to KrasG12C inhibition. *Clin. Cancer Res.* **26**, 1617–1643 (2020).
6. Solanki, H. S. *et al.* Cell type-specific adaptive signaling responses to KRASG12Cinhibition. *Clin. Cancer Res.* **27**, (2021).
7. Tong, X. *et al.* Adeno-to-squamous transition drives resistance to KRAS inhibition in LKB1 mutant lung cancer. *Cancer Cell* **42**, (2024).
8. Li, Z. *et al.* Alveolar Differentiation Drives Resistance to KRAS Inhibition in Lung Adenocarcinoma. *Cancer Discov.* **14**, (2024).
9. Singhal, A. *et al.* A Classical Epithelial State Drives Acute Resistance to KRAS Inhibition in Pancreatic Cancer. *Cancer Discov.* **14**, 2122–2134 (2024).
10. Narod, S. A. BRCA mutations in the management of breast cancer: The state of the art. *Nature Reviews Clinical Oncology* vol. 7 (2010).
11. Neff, R. T., Senter, L. & Salani, R. BRCA mutation in ovarian cancer: Testing, implications and treatment considerations. *Therapeutic Advances in Medical Oncology* vol. 9 (2017).
12. Castro, E. & Eeles, R. The role of BRCA1 and BRCA2 in prostate cancer. *Asian Journal of Andrology* vol. 14 (2012).
13. Greer, J. B. & Whitcomb, D. C. Role of BRCA1 and BRCA2 mutations in pancreatic cancer. *Gut* vol. 56 (2007).
14. Russo, M. *et al.* Adaptive mutability of colorectal cancers in response to targeted therapies. *Science (80-.).* **366**, (2019).
15. Maertens, O. *et al.* MAPK pathway suppression unmasks latent dna repair defects and confers a chemical synthetic vulnerability in BRAF-, NRAS-, and NF1 -mutant melanomas. *Cancer Discov.* **9**, (2019).
16. Ali, M. *et al.* Small-molecule targeted therapies induce dependence on DNA double-strand break repair in residual tumor cells. *Sci. Transl. Med.* **14**, (2022).
17. Dharanipragada, P. *et al.* Blocking Genomic Instability Prevents Acquired Resistance to

MAPK Inhibitor Therapy in Melanoma. *Cancer Discov.* (2023) doi:10.1158/2159-8290.cd-22-0787.

18. Russo, M. *et al.* A modified fluctuation-test framework characterizes the population dynamics and mutation rate of colorectal cancer persister cells. *Nat. Genet.* **54**, (2022).
19. Santana-Codina, N. *et al.* Defining and Targeting Adaptations to Oncogenic KRASG12C Inhibition Using Quantitative Temporal Proteomics. *Cell Rep.* **30**, 4584-4599.e4 (2020).
20. Certo, M. T. *et al.* Tracking genome engineering outcome at individual DNA breakpoints. *Nat. Methods* **8**, (2011).
21. Xue, J. Y. *et al.* Rapid non-uniform adaptation to conformation-specific KRAS(G12C) inhibition. *Nature* **577**, 421–425 (2020).
22. Oki, T. *et al.* A novel cell-cycle-indicator, mVenus-p27K -, identifies quiescent cells and visualizes G0-G1 transition. *Sci. Rep.* **4**, (2014).
23. Tsai, Y. S. *et al.* Rapid idiosyncratic mechanisms of clinical resistance to KRAS G12C inhibition. *J. Clin. Invest.* **132**, (2022).
24. Amodio, V. *et al.* EGFR Blockade Reverts Resistance to KRASG12C Inhibition in Colorectal Cancer. *Cancer Discov.* **10**, 1129–1139 (2020).
25. Olivieri, M. *et al.* A Genetic Map of the Response to DNA Damage in Human Cells. *Cell* **182**, (2020).
26. Subramanian, A. *et al.* A Next Generation Connectivity Map: L1000 Platform and the First 1,000,000 Profiles. *Cell* **171**, 1437-1452.e17 (2017).
27. Vallejo, A. *et al.* An integrative approach unveils FOSL1 as an oncogene vulnerability in KRAS-driven lung and pancreatic cancer. *Nat. Commun.* **8**, 14294 (2017).
28. Klomp, J. A. *et al.* Defining the KRAS-and ERK-dependent transcriptome in KRAS-mutant cancers. doi:10.1126/science.adk0775.
29. Erice, O. *et al.* LAMC2 Regulates Key Transcriptional and Targetable Effectors to Support Pancreatic Cancer Growth. *Clin. Cancer Res.* **29**, (2023).
30. Vallejo, A. *et al.* FOSL1 promotes cholangiocarcinoma via transcriptional effectors that could

be therapeutically targeted. *J. Hepatol.* **75**, (2021).

31. Fekete, J. T. & Győrffy, B. ROCplot.org: Validating predictive biomarkers of chemotherapy/hormonal therapy/anti-HER2 therapy using transcriptomic data of 3,104 breast cancer patients. *Int. J. Cancer* **145**, (2019).
32. Korach, J. *et al.* Long-term tolerability of olaparib tablets as maintenance therapy for platinum-sensitive relapsed ovarian cancer (PSR OC): Phase III SOLO2 trial. *Ann. Oncol.* **29**, (2018).
33. Mateo, J. *et al.* A decade of clinical development of PARP inhibitors in perspective. *Ann. Oncol.* **30**, (2019).
34. Li, P. *et al.* OFD1 inhibition induces BRCAness to create a therapeutic vulnerability to PARP inhibition in pancreatic cancer. *Nat. Commun. 2025 161* **16**, 1–18 (2025).
35. Kaplan, A. R. *et al.* Cediranib suppresses homology-directed DNA repair through down-regulation of BRCA1/2 and RAD51. *Sci. Transl. Med.* **11**, (2019).
36. Sun, C. *et al.* Rational combination therapy with PARP and MEK inhibitors capitalizes on therapeutic liabilities in RAS mutant cancers. *Sci. Transl. Med.* **9**, (2017).
37. Zatreanu, D. *et al.* Polθ inhibitors elicit BRCA-gene synthetic lethality and target PARP inhibitor resistance. *Nat. Commun.* **12**, (2021).
38. Seed, G. *et al.* Elucidating acquired PARP inhibitor resistance in advanced prostate cancer. *Cancer Cell* **42**, 2113-2123.e4 (2024).
39. Wu, Y., Song, Y., Wang, R. & Wang, T. Molecular mechanisms of tumor resistance to radiotherapy. *Molecular Cancer* vol. 22 (2023).
40. Song, D. *et al.* Blocking Fra-1 sensitizes triple-negative breast cancer to PARP inhibitor. *Cancer Lett.* **506**, (2021).
41. Holderfield, M. *et al.* Concurrent inhibition of oncogenic and wild-type RAS-GTP for cancer therapy. *Nature* **629**, (2024).
42. Jiang, J. *et al.* Translational and Therapeutic Evaluation of RAS-GTP Inhibition by RMC-6236 in RAS-Driven Cancers. doi:10.1158/2159-8290.CD-24-0027.

43. Tibor Fekete, J. & Győrffy, B. A unified platform enabling biomarker ranking and validation for 1562 drugs using transcriptomic data of 1250 cancer cell lines. *Comput. Struct. Biotechnol. J.* **20**, (2022).
44. Gentleman, R. C. *et al.* Bioconductor: open software development for computational biology and bioinformatics. *Genome Biol.* **5**, (2004).
45. Ritchie, M. E. *et al.* Limma powers differential expression analyses for RNA-sequencing and microarray studies. *Nucleic Acids Res.* **43**, (2015).
46. Ge, S. X., Jung, D., Jung, D. & Yao, R. ShinyGO: A graphical gene-set enrichment tool for animals and plants. *Bioinformatics* **36**, (2020).
47. Hao, Y. *et al.* Dictionary learning for integrative, multimodal and scalable single-cell analysis. *Nat. Biotechnol.* **42**, (2024).
48. Love, M. I., Huber, W. & Anders, S. Moderated estimation of fold change and dispersion for RNA-seq data with DESeq2. *Genome Biol.* **15**, (2014).
49. Wilkinson, L. ggplot2: Elegant Graphics for Data Analysis by WICKHAM, H. *Biometrics* **67**, (2011).

FUNDING SOURCES

S.V. is supported by a Project PID2023-152755OB-I00 funded by MICIU/AEI/10.13039/501100011033 and FEDER, UE, by Worldwide Cancer Research (25-0196), by the Department of Health of the Government of Navarre within the framework of the call for proposals for research projects (project code: GN2024/01), and by donations from Maria Eugenia Burgos de la Iglesia's family and the Baringo family. S.V. was also funded by the Government of Navarra and ''Fondo Europeo de Desarrollo Regional (FEDER)'' (project: 0011-1411-2025-000111; NAIARA). J.J.J-A. is supported by a postdoctoral fellow (POSTD246238JIME) and a SINERGIA project (SNRGS259722JIME) from the Foundation of the Spanish Association Against Cancer (AECC). R.P-C. is supported by a SINERGIA project (SNRGS247052PRAD_SNRGS24) from the Foundation of the Spanish Association Against Cancer (AECC). T.M. is supported by grants from

the Spanish Institute of Carlos III (PI20/00898, PI24/00526, FORT23/00034). F.L. is supported by a project from MICIU PID2024-156335OB-100 funded by MICIU/AEI/10.13039/501100011033 and FEDER, UE. This study was also supported by CIBERONC (CB16/12/00443). A.B. is supported by European Research Council (ERC) under the European Union's Horizon 2020 research and innovation programme (TARGET, grant agreement n. 101020342) (A.B.); AIRC under 5 per Mille 2018 - ID. 21091 program – P.I. Bardelli Alberto (A.B.); IMI contract n. 101007937 PERSIST-SEQ (A.B.); AIRC under IG 2023 - ID. 28922 project – P.I. Bardelli Alberto (A.B.). Views and opinions expressed are however those of the author(s) only and do not necessarily reflect those of the European Union or the European Research Council. Neither the European Union nor the granting authority can be held responsible for them. T.V.T. is supported by grants from the Spanish Ministry of Science, Innovation and Universities (PID2023-146827OB-I00), "Ramon y Cajal" program (RYC2020-029098-I). M.R. is supported by AIRC under MFAG 2021-ID 26439 project – PI M.R.; PNRR M4C2-Investimento 1.4-CN00000041 "Finanziato dall'Unione Europea-NextGenerationEU" (M.R.).

AUTHOR CONTRIBUTIONS

Conceptualization: C.W. and S.V. Investigation: C.W., G.N-J., C.V., I.M., J.J.J-A., A.S., A.F-L., S.L., M.J., R.P-C., H.M., I.L., N.B., J.R., A.C.D., P.B., X.B-C. and E.G. Data curation: C.W., E.G., T.V.T., I.F., M.R., and S.V. Formal analysis: C.W., G.N-J., C.V., I.M., E.G., A.C., M.R. and S.V. Computational analysis: X.B-C., P.B., E.G., and G.C. Resources: T.M., L.P-A., J.J., T.T., R.M-M., F.L., A.B., T.V.T., I.F., M.R., and S.V. Supervision: I.F., T.V.T., M.R., and S.V. Writing of the original draft: C.W. and S.V. Writing, review and editing: all authors.

DECLARATION OF INTERESTS

S.V. has received research funding unrelated to this project and consulting fees from Revolution Medicines, additional funding for unrelated work from Roche, Verastem Oncology, and BridgeBio, and is a scientific advisor for Libera Bio. F.L. has received funding for unrelated work

from Roche. A.B. reports receipt of grants/research supports from Neophore. A.B. is stock shareholder of Neophore and Kither Biotech. A.B. is advisory boards member for Neophore.

FIGURES

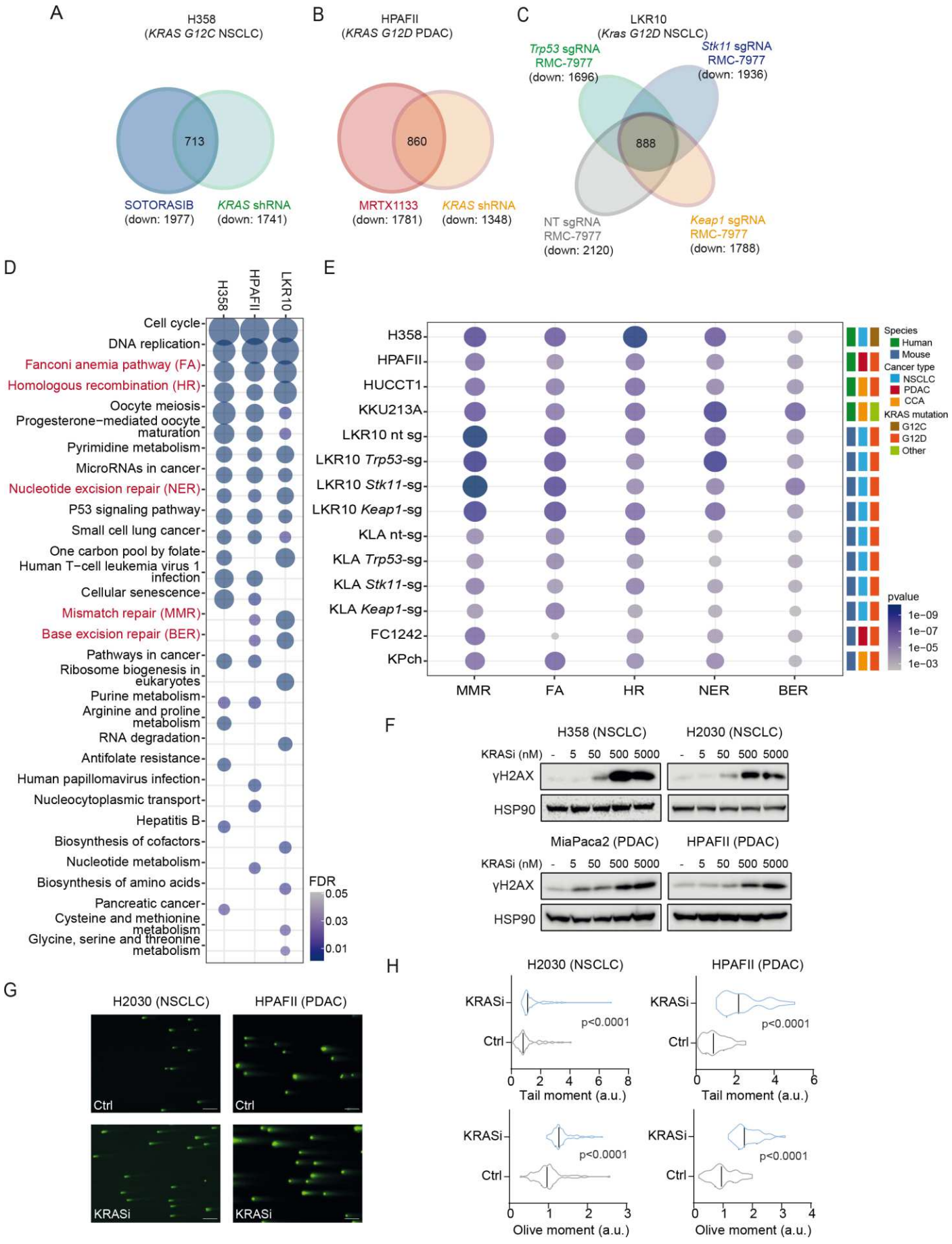

A
H358
(KRAS G12C NSCLC)
713
SOTORASIB
(down: 1977)
KRAS shRNA
(down: 1741)
B
HPAFII
(KRAS G12D PDAC)
860
MRTX1133
(down: 1781)
KRAS shRNA
(down: 1348)
C
LKR10
(Kras G12D NSCLC)
Trp53 sgRNA
RMC-7977
(down: 1696)
Stk11 sgRNA
RMC-7977
(down: 1936)
888
NT sgRNA
RMC-7977
(down: 2120)
Keap1 sgRNA
RMC-7977
(down: 1788)
D
H358
HPAFII
LKR10
Cell cycle
DNA replication
Fanconi anemia pathway (FA)
Homologous recombination (HR)
Oocyte meiosis
Progesterone−mediated oocyte maturation
Pyrimidine metabolism
MicroRNAs in cancer
Nucleotide excision repair (NER)
P53 signaling pathway
Small cell lung cancer
One carbon pool by folate
Human T−cell leukemia virus 1 infection
Cellular senescence
Mismatch repair (MMR)
Base excision repair (BER)
Pathways in cancer
Ribosome biogenesis in eukaryotes
Purine metabolism
Arginine and proline metabolism
RNA degradation
Antifolate resistance
Human papillomavirus infection
Nucleocytoplasmic transport
Hepatitis B
Biosynthesis of cofactors
Nucleotide metabolism
Biosynthesis of amino acids
Pancreatic cancer
Cysteine and methionine metabolism
Glycine, serine and threonine metabolism
FDR
0.05
0.03
0.01
E
H358
HPAFII
HUCCT1
KKU213A
LKR10 nt sg
LKR10 Trp53-sg
LKR10 Stk11-sg
LKR10 Keap1-sg
KLA nt-sg
KLA Trp53-sg
KLA Stk11-sg
KLA Keap1-sg
FC1242
KPch
MMR
FA
HR
NER
BER
Species
Human
Mouse
Cancer type
NSCLC
PDAC
CCA
KRAS mutation
G12C
G12D
Other
pvalue
1e−09
1e−07
1e−05
1e−03
F
H358 (NSCLC)
H2030 (NSCLC)
KRASi (nM) - 5 50 500 5000
γH2AX
HSP90
MiaPaca2 (PDAC)
HPAFII (PDAC)
G
H2030 (NSCLC)
HPAFII (PDAC)
Ctrl
KRASi
H
H2030 (NSCLC)
HPAFII (PDAC)
KRASi
Ctrl
p<0.0001
Tail moment (a.u.)
Olive moment (a.u.)

Figure 1. KRAS inhibition induces DNA damage repair deficiency. A. Common downregulated genes in H358 cells exposed to pharmacological (1 μM Sotorasib, 24 hours) or genetic (shRNA) KRAS inhibition compared to controls (vehicle and GFP shRNA) (log2FC<1; B>0). **B.** Common downregulated genes in HPAFII cells exposed to pharmacological (1 μM MRTX1133, 24 hours) or genetic (shRNA) KRAS inhibition compared to controls (vehicle and GFP shRNA) (log2FC<1; B>0). **C.** Common downregulated genes in mouse isogenic LKR10 cells CRISPR-edited for *Trp53*, *Stk11* or *Keap1* genes, and exposed to RAS(ON) multi-selective inhibitor RMC-7977 (1 μM) for 24 hours. NT: non-targeted sgRNA. **D.** Gene Ontology analysis of biological pathways from downregulated genes in A, B and C using ShinyGo. Circle size relative to the number of genes in a specific biological pathway. **E.** Negative enrichment of DDR related biological pathways (mismatched repair: MMR; Fanconi Anemia: FA; homologous recombination: HR; nucleotide excision repair: NER; base excision repair: BER) in the RNA expression data of human and mouse cell lines from NSCLC, PDAC and CCA under pharmacological KRAS inhibition (sotorasib: H358; MRTX1133: HPAFII; RMC-7977: HUCCT1, KKU-213A, LKR10 nt-sgRNA, LKR10 *Trp53*-sgRNA, LKR10 *Stk11*-sgRNA, LKR10 *Keap1*-sgRNA, KLA nt-sgRNA, LKR10 *Trp53*-sgRNA, KLA *Stk11*-sgRNA, KLA *Stk11*-sgRNA, FC1242, and KPch). Circle size and colour are indicative of the p value. **F.** γH2AX protein expression in H358, H2030, MiaPaca2 and HPAFII cell lines after 48 h of increasing KRASi concentration treatment (loading control: HSP90). **G.** Representative neutral comet assay images of H2030 and HPAFII cell lines after 48 hour-treatment with vehicle and KRASi (H2030: 150 nM; HPAFII: 50 nM) treatment. Scale bar: 100 μm **H.** Quantification of the tail and olive moment of comet assay images in G (a.u.: arbitrary units).

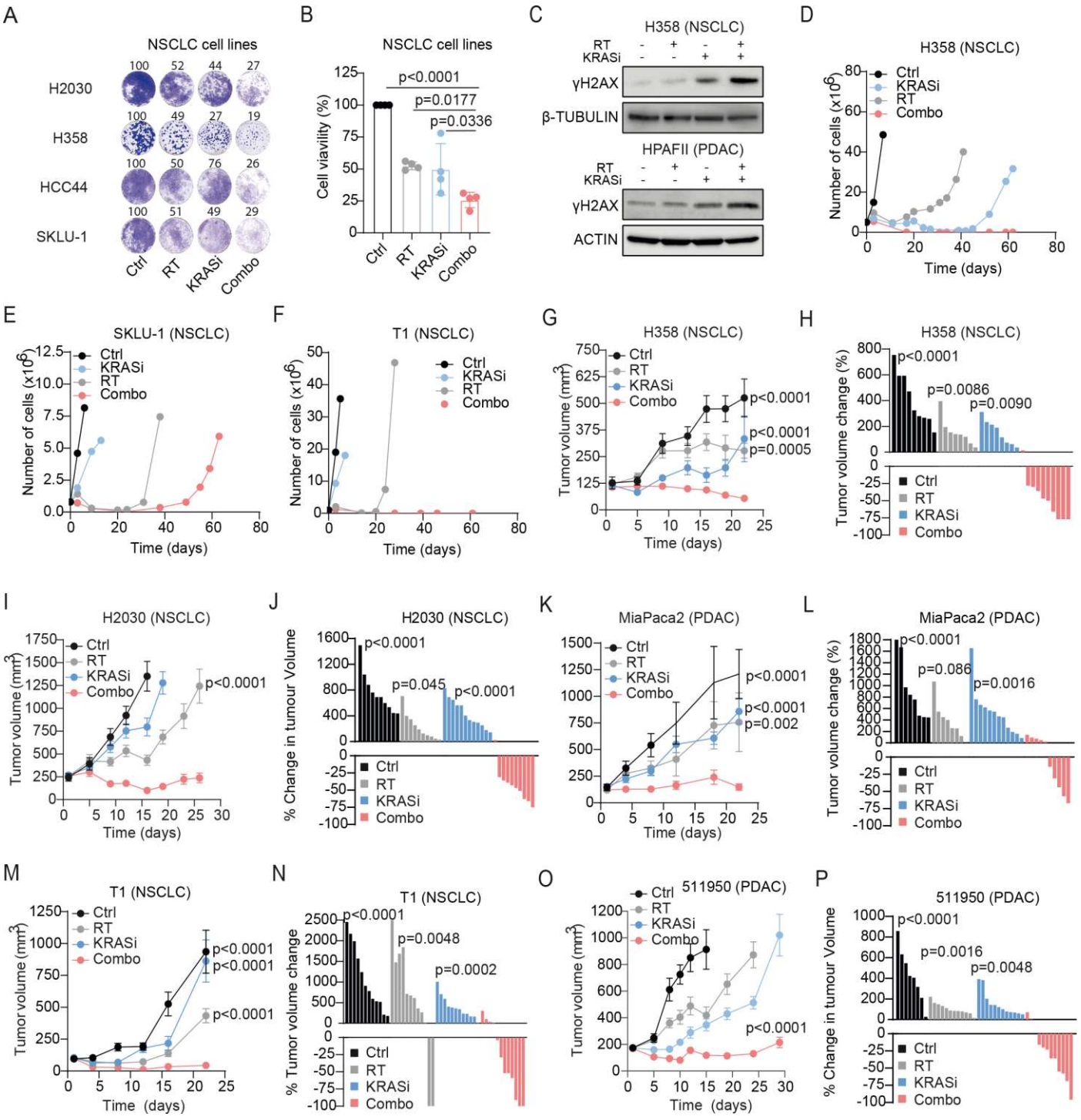


Figure 2. Synergistic antitumor effect of radiotherapy and KRASi in mut *KRAS* NSCLC and PDAC cell lines. A. Representative crystal violet staining images of H2030, H358, HCC44 and SKLU-1 cell lines treated with a single dose of RT (2-4 Gy) and a KRASi (Soto: 40-80 nM, MRTX1133: 400 nM) for 5 days. **B.** Quantification of data from A (data: mean +/- SD; test: one-way ANOVA, Tukey's adjustment). **C.** γH2AX protein expression in H358 and HPAFII cell lines after 48 hours of RT (1 Gy) and KRASi (sotorasib: 10 nM; MRTX1133: 50 nM) treatment (loading control: β-TUBULIN and ACTIN). **D-F.** Growth of H358 (D), SKLU-1 (E) and T1 (F) cells upon indicated

treatments (RT: 5, 10 and 20 Gy respectively; KRASi: 0.05 µM sotorasib, 5 µM MRTX1133, and 2,5 µM sotorasib, respectively) until the emergence of resistance (n = 1 biological experiment). **G.** Growth kinetics of H358 cell-derived subcutaneous tumors upon indicated treatments (RT: 15 Gy; KRASi: 10 mg/kg). N= 8-9 tumors per group in $Rag2^{-/-}$; $Il2\gamma r^{-/-}$ mice (data: mean +/- SEM; test: two-way ANOVA, Tukey's multiple comparisons). **H.** Waterfall plots of tumors from G (H358) at the last day of experiment represented as percent tumor volume fold change (data: mean +/- SEM; test: one-way ANOVA). **I.** Growth kinetics of H2030 cell-derived subcutaneous tumors upon indicated treatments (RT: 20 Gy; KRASi: 30 mg/kg). N= 10-12 tumors per group in $Rag2^{-/-}$; $Il2\gamma r^{-/-}$ mice (data: mean +/- SEM; test: two-way ANOVA, Tukey's multiple comparisons). **J.** Waterfall plots of tumors from I (H2030) at day 16 of experiment represented as percent tumor volume fold change (data: mean +/- SEM; test: one-way ANOVA). **K.** Growth kinetics of MiaPaca2 cell-derived tumors upon indicated treatments (RT: 15 Gy; sotorasib: 10 mg/kg). N= 8-12 tumors per group in $Rag2^{-/-}$; $Il2\gamma r^{-/-}$ mice (data: mean +/- SEM; test: two-way ANOVA, Tukey's multiple comparisons). **L.** Waterfall plots of tumors from K (MiaPaca2) at the last day of experiment represented as percent tumor volume fold change (data: mean +/- SEM; test: Kruskal Wallis). **M.** Growth kinetics of T1 cell-derived subcutaneous tumors upon indicated treatments (RT: 15 Gy; sotorasib: 30 mg/kg). N= 12 tumors per group in F1 C57BL/6 x 129S4/Sv immunocompetent mice (data: mean +/- SEM; test: two-way ANOVA, Tukey's multiple comparisons). **N.** Waterfall plots of tumors from M (T1) at the last day of experiment represented as percent tumor volume fold change (data: mean +/- SEM; test: Kruskal Wallis). **O.** Growth kinetics of 511950 cell-derived subcutaneous tumors upon indicated treatments (RT: 15 Gy; MRTX1133: 30 mg/kg twice daily). N= 8-12 tumors per group in F1 C57BL/6 x 129S4/Sv immunocompetent mice (data: mean +/- SEM; test: two-way ANOVA, Tukey's multiple comparisons). **P.** Waterfall plots of tumors from O (511950) at the last day of experiment represented as percent tumor volume fold change (data: mean +/- SEM; test: Kruskal Wallis).

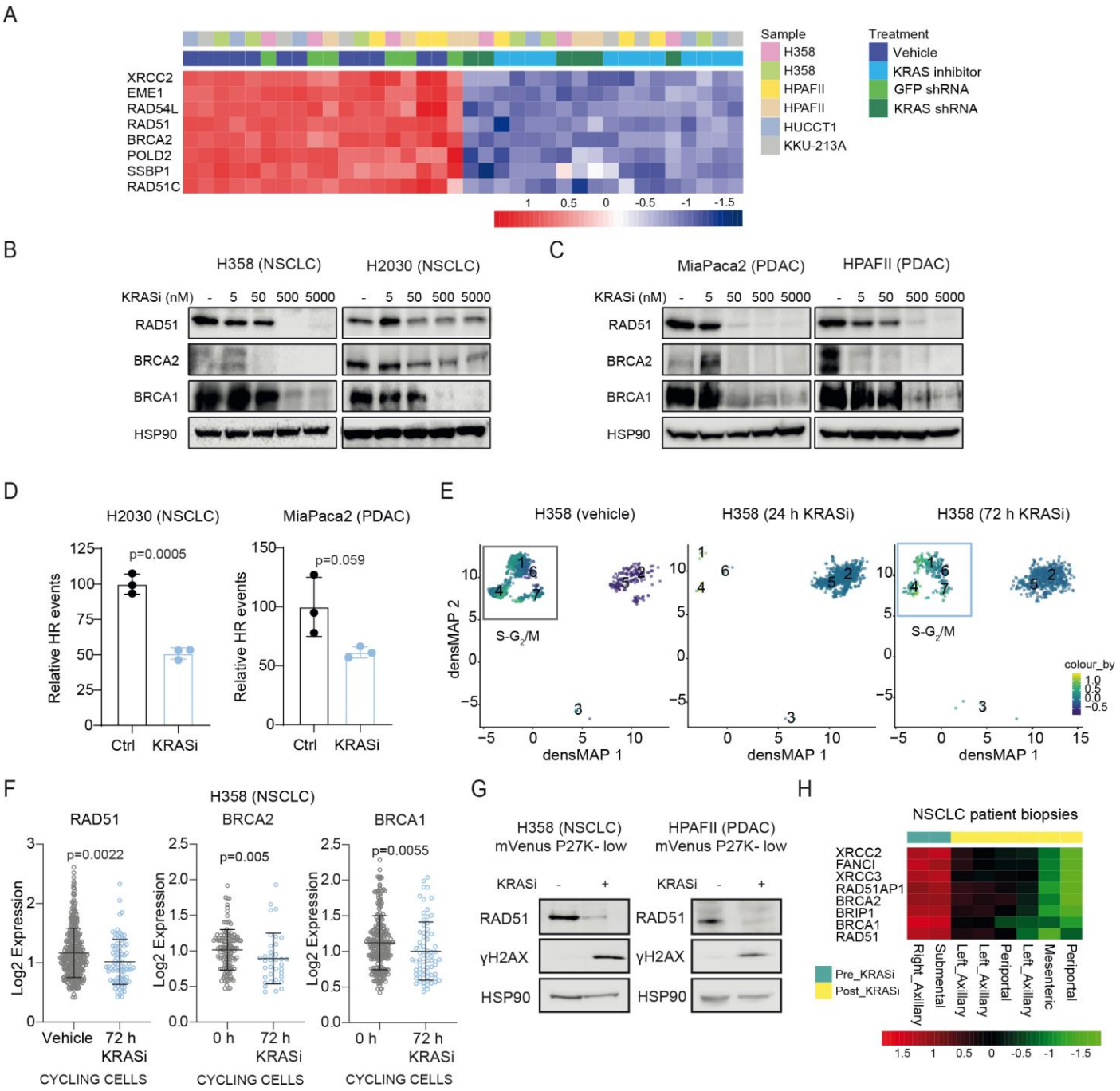


Fig. 3. KRASi induces a homologous recombination deficiency state in drug-tolerant populations. A. Heat map of RNA normalized expression of HR genes in human mut *KRAS* NSCLC (H358), PDAC (HPAFII) and CCA (HUCCT1, KKU-213A) cell lines subjected to genetic or pharmacological KRAS inhibition (log2FC<-1, p<0.05). **B and C.** Immunoblot analysis of RAD51, BRCA2 and BRCA1 protein expression in NSCLC (H358 and H2030, B) and PDAC (MiaPaca2 and HPAFII, C) cell lines exposed to increasing KRASi (sotorasib and MRTX1133) concentrations for 48 hours (loading control: HSP90). **D.** Relative HR events in NSCLC (H2030) and PDAC (MiaPaca2) cell lines transduced with the triplasmid construct traffic light reporter (TLR) system. Homologous

recombination (HR) events were measured and quantified by flow cytometry after 72 hours of vehicle or KRASi treatment (1 μM) (data: mean +/- SD; test: Student-t). **E.** Single-cell scatter plots of *in vitro* scRNA-seq data[21] from H358 cells treated with KRASi (10 μM ARS1620) for 0, 24 and 72 hours. Cell clustering is based on expression of genes related to cell cycle phases. Squares highlight proliferating cells in S-G_2/M (method: densMAP). **F.** Expression of HR genes BRCA1/2 and RAD51 in data from E (data: mean +/- SD; test: Student-t). **G.** RAD51 and γH2AX protein expression in the cycling populations of HPAFII cells (mVenus P27K low) treated with vehicle or KRASi (MRTX1133: 200 nM) for 72 hours (loading control: HSP90). **H.** Heat map of RNA expression of HR genes in lymph node biopsies derived from a NSCLC patient either before (pretreatment) or after (posttreatment) exposure to a KRASi (sotorasib)[23] (log2FC<1; $p<0.05$).

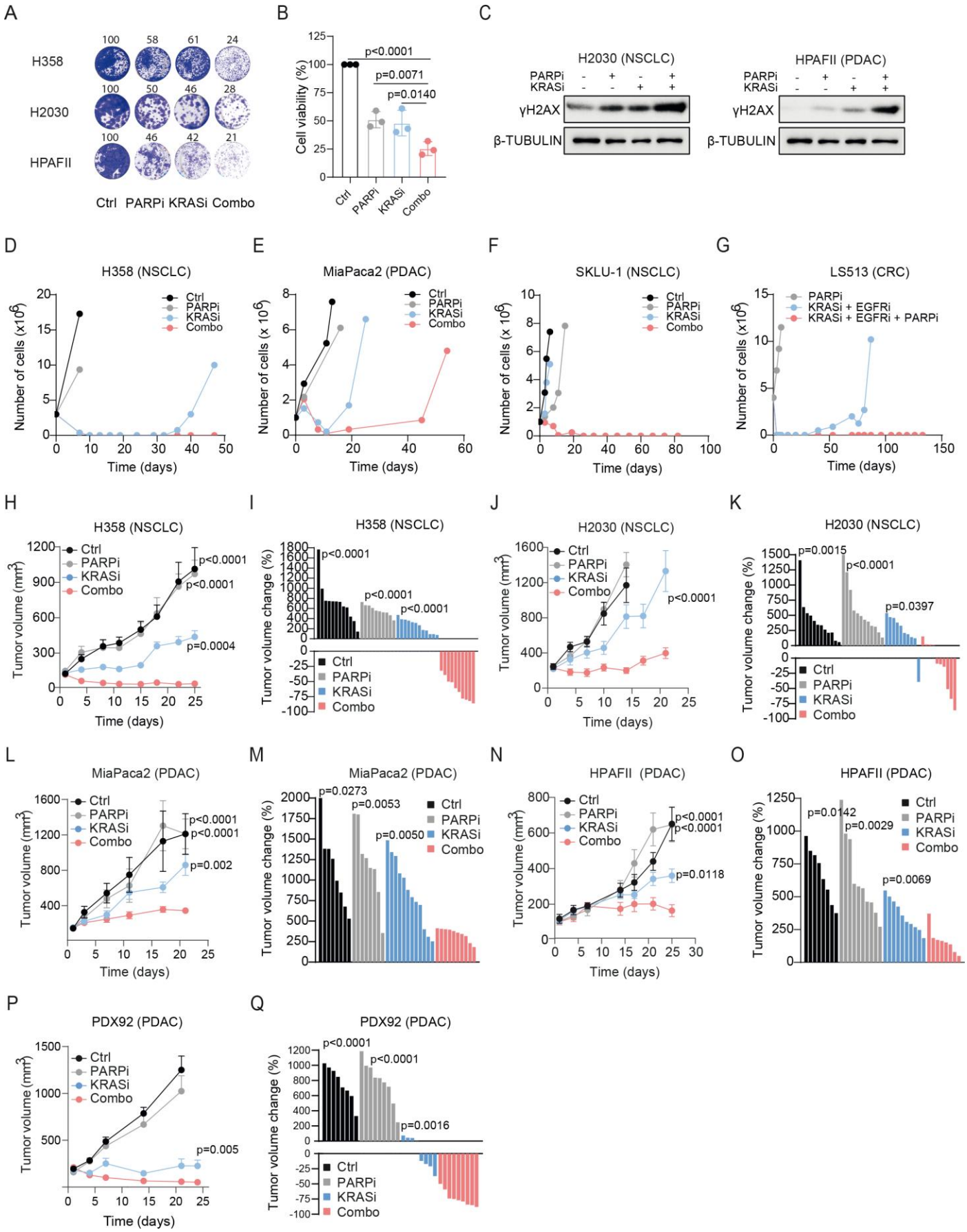


Figure 4. Synergistic antitumor effect of PARPi and KRASi in mut *KRAS* LUAD and PDAC cell lines. A. Representative crystal violet staining images of 10-day treatment (control: Ctrl; PARPi: 2.5

μM; KRASi: 5-12.5 nM) of H358, H2030 and HPAFII cell lines. **B.** Long-term effect of PARPi and KRASi combination on cell viability of *KRAS* mutant cells (H358, H2030 and HPAFII). 10-day treatment (data: mean +/- SD; test: one-way ANOVA, Tukey's adjustment). **C.** γH2AX protein expression in H2030 and HPAFII cell lines after 48 h of PARPi (5 μM) and KRASi (50 nM) treatment (loading control: β-Tubulin). **D-G.** Growth of H358 (D), MiaPaca2 (E), SKLU-1 (F) and LS513 (G) cells treated with indicated drugs (PARPi: 5 μM; KRASi: 0.1, 0.5, 5 and 0.1 μM respectively; EGFRi (cetuximab: CTX): 50 μg/mL) until the emergence of resistance (n = 1 biological experiment). **H.** Growth kinetics of H358 cell-derived subcutaneous tumors treated with indicated drugs (PARPi: 50 mg/Kg; KRASi: 10 mg/kg). N= 10-12 tumors per group in $Rag2^{-/-}$; $Il2\gamma r^{-/-}$ mice (data: mean +/- SEM; test: two-way ANOVA, Tukey's multiple comparisons). **I.** Waterfall plots of tumors from H (H358) at the last day of experiment represented as percent tumor volume fold change (test: Brown Forsythe and Welch ANOVA). **J.** Growth kinetics of H2030 cell-derived subcutaneous tumors treated with indicated drugs (PARPi: 50 mg/kg; KRASi: 30 mg/Kg). N= 10-12 tumors per group in $Rag2^{-/-}$; $Il2\gamma r^{-/-}$ mice (data: mean +/- SEM; test: two-way ANOVA, Sidak's multiple comparisons). **K.** Waterfall plots of tumors from J (H2030) at day 14 of experiment represented as percent tumor volume change (test: Kruskal-Wallis). **L.** Growth kinetics of MiaPaca2 cell-derived subcutaneous tumors treated with indicated drugs (PARPi: 50 mg/Kg; KRASi: 10 mg/kg). N= 8-12 tumors per group in $Rag2^{-/-}$; $Il2\gamma r^{-/-}$ mice (data: mean +/- SEM; test: two-way ANOVA, Sidak's multiple comparisons). **M.** Waterfall plots of tumors from L (MiaPaca2) at the last day of experiment represented as percent tumor volume fold change (test: Brown Forsythe and Welch ANOVA). **N.** Growth kinetics of HPAFII cell-derived subcutaneous tumors treated with indicated drugs (PARPi: 50 mg/Kg; KRASi: 10 mg/Kg). N= 8-10 tumors per group in $Rag2^{-/-}$; $Il2\gamma r^{-/-}$ mice (data: mean +/- SEM; test: two-way ANOVA, Tukey's multiple comparisons). **O.** Waterfall plots of tumors from N (HPAFII) at the last day of experiment represented as percent tumor volume fold change (test: Brown Forsythe and Welch ANOVA). **P.** Growth kinetics of PDX92-derived subcutaneous tumors treated with indicated drugs (PARPi: 100 mg/Kg; KRASi: 10 mg/kg). N= 8-10 tumors per group in $Rag2^{-/-}$; $Il2\gamma r^{-/-}$ mice (data: mean +/- SEM; test: two-way ANOVA, Sidak's multiple comparisons). **Q.** Waterfall plots of tumors from P (PDX92)

at the last day of experiment represented as percent tumor volume fold change (test: Brown Forsythe and Welch ANOVA).

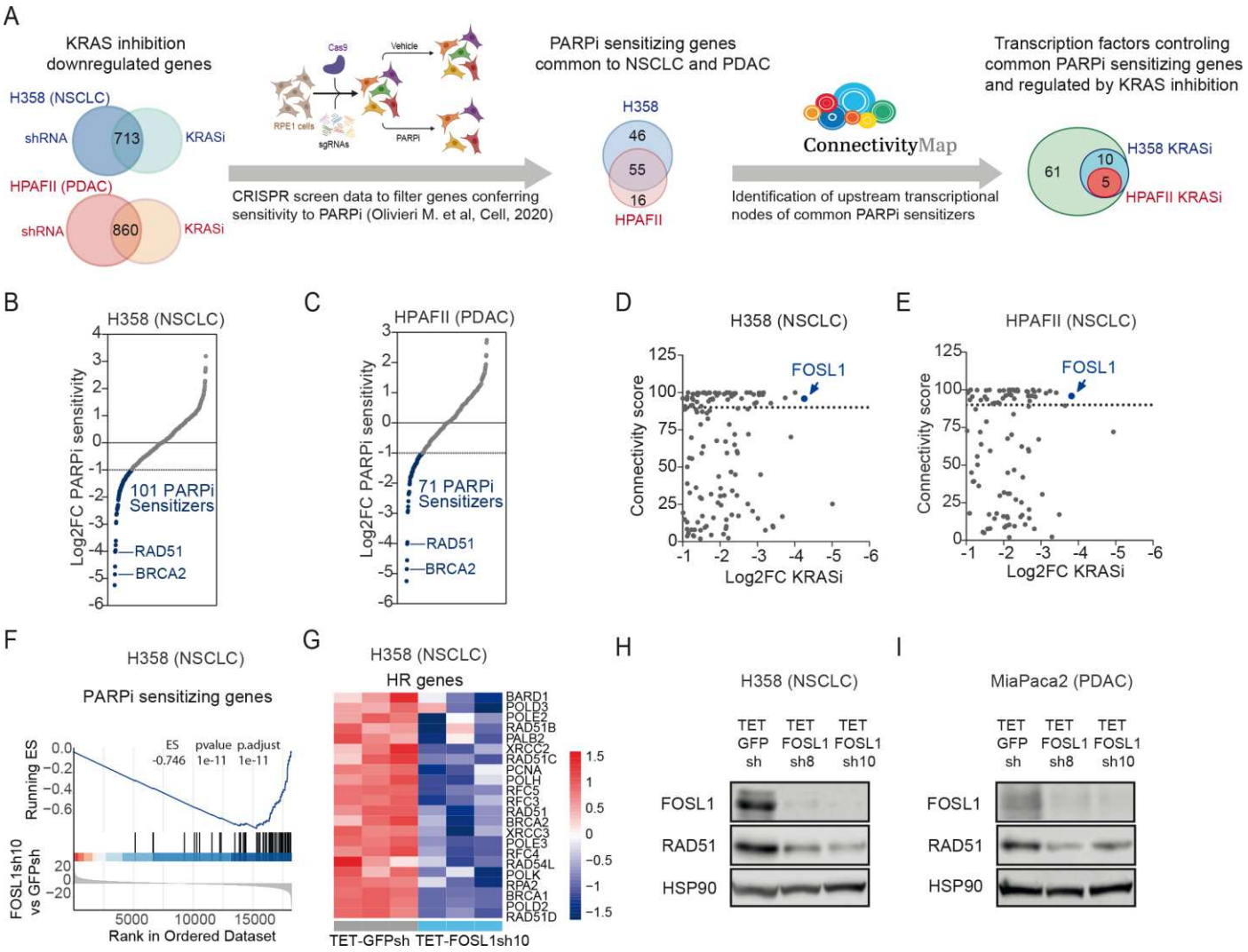


Figure 5. Identification of functional nodes linking KRAS to the homologous recombination machinery. A. Workflow of the integrative strategy to identify KRAS-regulated transcriptional nodes functionally involved in the response to PARPi. **B and C.** Genes commonly regulated by KRAS from either NSCLC (H358, B) or PDAC (HPAFII, C) cells undergoing pharmacological or genetic KRAS inhibition (Log2FC<-0.5, P<0.05) and contrasted against a genome-wide CRISPR screen to identify PARPi sensitizers[25] (Log2FC<-1). **D and E.** Graphs integrating upstream transcriptional regulators of the genes identified in B (NSCLC, D) and C (PDAC, E) and expression data from the corresponding KRASi-treated cell lines. **F.** Gene set analysis of PARPi sensitizing genes projected into a ranked-ordered list of transcriptomics data from H358 cell line expressing a FOSL1 tetracycline-inducible shRNA (TET-shRNA FOSL1) vs the control condition (TET-shRNA GFP). **G.** Heat map of homologous recombination (HR) genes downregulated upon FOSL1 genetic inhibition with a specific shRNA (Log_2FC <-1, P<0.05). **H and I.** Immunoblot analysis of HR protein RAD51 in

NSCLC (H358) and PDAC (MiaPaca2) cell lines expressing a TET-inducible control GFP or two independent FOSL1 shRNAs (loading control: HSP90).

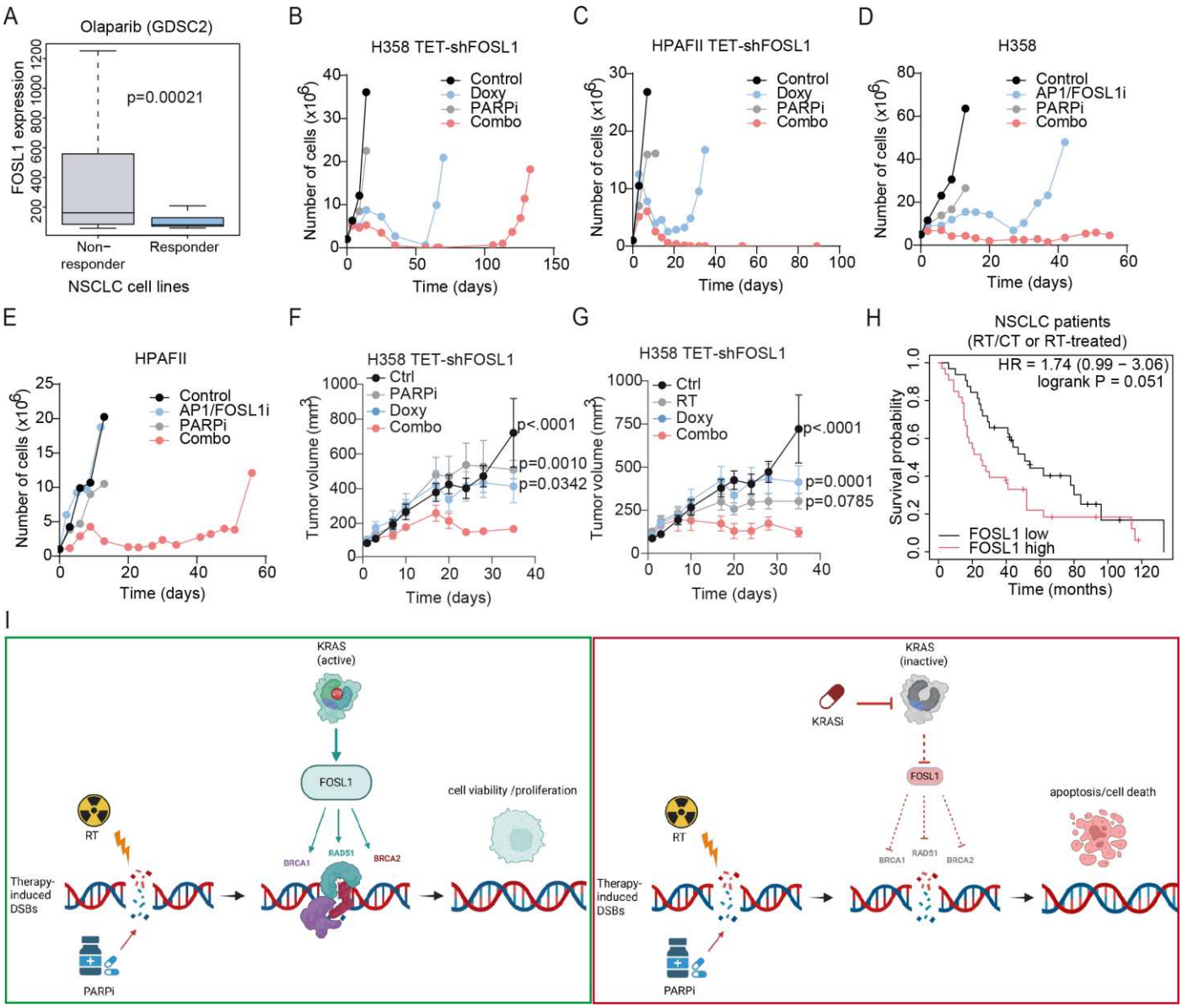


Figure 6. FOSL1 genetic inhibition renders NSCLC and PDAC sensitive to DNA damaging therapies. A. FOSL1 gene expression in responders and non-responders NSCLC cell lines to olaparib (PARPi) treatment. Data obtained from Genomics of Drug Sensitivity in Cancer study (version 2) at ROCplotter.org[31] (data: median ± 95% CI; test: ROC). **B-C.** Growth of H358 TET-FOSL1sh (B) and HPAFII TET-FOSL1sh (C) cells treated with indicated drugs (Doxy: 2 mg/mL; PARPi: 5 μM) until the emergence of resistance (n = 1 biological experiment). **D-E.** Growth of H358 (D) and HPAFII (E) cells treated with indicated drugs (AP1/FOSL1i T-5224: 7.5 μM; PARPi: 5 μM) until the emergence of resistance (n = 1 biological experiment). **F.** Growth kinetics of H358 TET-FOSL1sh cell-derived subcutaneous tumors treated with indicated drugs (PARPi: 50 mg/kg; doxy: 2 mg/mL). N= 8-12 tumors per group in Rag2$^{-/-}$; Il2γr$^{-/-}$ mice (data: mean +/- SEM; test: two-way

ANOVA, Tukey's multiple comparisons). **G.** Growth kinetics of H358 TET-FOSL1sh cell-derived subcutaneous tumors upon indicated treatments (RT: 15 Gy; doxy: 2 mg/mL). N= 6-10 tumors per group in $Rag2^{-/-}$; $Il2\gamma r^{-/-}$ mice (data: mean +/- SEM; test: two-way ANOVA, Tukey's multiple comparisons). **H.** Kaplan-Meier plot showing overall survival of NSCLC patients treated with RT or RT-chemotherapy (CT) as a function of FOSL1 expression (test: Logrank) using KM plotter. **I.** Graphical scheme showing how DNA damaging therapies synergize with KRAS inhibitors which induce DNA damage repair deficiency, in mutant *KRAS* LUAD and PDAC tumors.

Supplementary Files

This is a list of supplementary files associated with this preprint. Click to download.

- WelchetalSupplementaryInformationv7.docx
- SupplTable1H358HPAFIILKR10RNAseq.xlsx
- SupplTable2HUCCT1KKU213AKPchFC1242KLARNAseq.xlsx
- SupplTable3LymphNodesRNAseq.xlsx
- SupplTable4IntegrativeAnalysis.xlsx